Journal of Non-Crystalline Solids 481 (2018) 225–238

Contents lists available at ScienceDirect

Journal of Non-Crystalline Solids

journal homepage: www.elsevier.com/locate/jnoncrysol

Self-cleaning and spectral attributes of erbium doped sodium-zinc-tellurite glass: Role of titania nanoparticles

N.N. Yusof[a], S.K. Ghoshal[a,*], R. Arifin[a], A. Awang[b], H.S. Tewari[c], K. Hamzah[d]

[a] Advanced Optical Materials Research Group, Physics Department, Faculty of Science, Universiti Teknologi Malaysia, 81300 Johor Bahru, Skudai, Malaysia
[b] Physics with Electronics Program, Faculty of Science and Natural Resources, Universiti Malaysia Sabah, 88400 Kota Kinabalu, Sabah, Malaysia
[c] Department of Pure and Applied Physics, Guru Ghasidas University, Bilaspur 495009, India
[d] Nuclear Engineering Programme, Faculty of Petroleum and Renewable Energy Engineering, Universiti Teknologi Malaysia, 81310 UTM Johor Bahru, Johor, Malaysia

ARTICLE INFO

Keywords:
Self-cleaning
Spectral features
Tellurite glass
Titania nanoparticles
Water contact angle
Photocatalytic

ABSTRACT

Highly transparent and durable self-cleaning materials became demanding for diverse applications. To attain such goals, glass system with composition $(69 - x)TeO_2$-20ZnO-10Na_2O-1Er_2O_3-$(x)TiO_2$, where $x = 0.0$, 0.1, 0.2, 0.3 and 0.4 mol% were synthesized using the conventional melt quenching method and characterized. For the first time, the influence of embedded TiO_2 (Titania) nanoparticles (TNPs) concentration variation on the self-cleaning and spectral properties was examined to establish their correlation. TEM micrograph revealed the nucleation of spherical TNPs (average size ≈ 14 nm) inside the amorphous matrix. Reduction in the optical band gap energy (from 3.08–3.03 eV) and water contact angle (from 68° to 43°) both were evidenced with the increase in TNPs contents, wherein the later one (reduced contact angle or enhanced wettability) was attributed to the enhanced hydrophilicity of the glass samples. Conversely, a slight increase in the methylene blue (MB) degradation rate with the increase of TNPs contents up to 0.2 mol% indeed indicated an improved photocatalytic activity of the synthesized glass. The absorption spectra exhibited ten significant bands of Er^{3+} ions in the wavelength range of 407 to 1532 nm. The emergent three prominent photoluminescence (PL) emission bands of the glass sample (with 0.2 mol% of TNPs) positioned at 535 nm, 555 nm and 670 nm were enhanced by a factor of 6.77, 4.56 and 2.00, respectively. Surface plasmon resonance (SPR) band of the embedded TNPs inside the glass was detected around 581 nm. Furthermore, Raman band of the glass (containing 0.4 mol% of TNPs) centred at 845 cm^{-1} displayed an intensity enhancement by a factor of 3.58 times, which was ascribed to the TNPs localized SPR field mediated effect. It is established that the measured enhanced hydrophilicity (self-cleanliness) and improved spectral features of the present glass composition was steered by the TNPs surface plasmon assisted effects.

1. Introduction

Inspired by the sustained natural acts shown by lotus leaf and butterfly wings, the self-cleaning technology received a great attention in late 20th century. Lately, extensive research efforts have been dedicated to develop highly efficient and durable self-cleaning coating surfaces with enhanced optical qualities [1–4]. The optical qualities of material are signified in terms of excellent transmittance of incident light [5], high refractive index [6], unique up-conversion (UC) ability to facilitate electronic transition and wide absorption capacity from UV to visible region [7]. These qualities are advantageous for multi-functional applications in optoelectronic and bio-photonic fields [8]. Glass systems having such attributes also may be useful for solar cell application where the efficiency of energy conversion can be enhanced via Er^{3+} ions doping inside the host glass [9]. Sustainable materials such as tiles [10], textiles [11–13] plastic [14] and glass [15,16] with self-cleaning properties were greatly demanded and thereby became commercially available (e.g. BalcoNano™ from Balcony Systems Solutions, Rain Racer™ from Rain Racer Developments, ClearShield™ from Ritec International) [1,17,18]. To protect glass surface from pollutants contamination empowered transparency lose various strategies were adopted [4,6]. Such taints on glass surface not only causes vision opacity but also accountable for considerable aesthetic damages of cultural heritage unless averted. In fact, the complex mechanism involving the clinging of ultrafine dirt particulates on wetting layers is poorly understood.

It is needless to say that among various self-cleaning materials, glass system owing to their extreme durability, thermal stability, and

* Corresponding author.
E-mail addresses: sibkrishna@utm.my (S.K. Ghoshal), ramliarifin@utm.my (R. Arifin), khaidzir@utm.my (K. Hamzah).

http://dx.doi.org/10.1016/j.jnoncrysol.2017.10.044
Received 1 August 2017; Received in revised form 20 October 2017; Accepted 23 October 2017
Available online 07 November 2017
0022-3093/

transparency have gained special attention in the building and construction industries, automotive sectors, optical devices, fuel-cells and solar panels [18,19]. Usage of these self-cleaning glass is rather interesting since it would lessen both the cleanliness maintenance time and cost, leading to more economical and environmental amiable material [18]. Besides, self-cleaning glass systems are viewed as innovative and efficient material for pollutant removal and energy production [20,21]. Earlier, self-cleaning glass systems were made by coating the glass surface with Titania (TiO_2) nanoparticles (TNPs) to induce photocatalytic activity and promote self-cleanliness. However, such glass is unable to maintain the prolonged self-cleanliness due to leaching problem associated with the coating material that often gets rid of easily from the glass surface. Meanwhile, TNPs in powder form can draw impurities into water during the photocatalytic reaction and thus additional extraction process is prerequisite to retrieve the TNPs in water treatment. To surmount such limitation, embedment of TNPs inside the glass matrix via chemical composition optimization appears more advantageous for large-scale pollutant removal and water purification applications. In-depth literature review revealed that development of self-cleaning glass system using a method other than coating of TNPs above the host surface is lacking [21].

Generally, the self-cleaning capability of materials is achieved by controlling their surface wettability [18], where the photocatalytic properties of the material play a paramount role [1,22]. Material's surface is considered as super-hydrophilic when the water contact angle (WCA) is below 50°. Conversely, the surface is categorized as super-hydrophobic when WCA is above 150° [23]. Instead of super-hydrophobic trait, super-hydrophilic characteristic is recognized as new way to create self-cleaning glass since a minimum angle of inclination is essential for a droplet to roll off the surface [4]. Photocatalysis being a chemical reaction between organic species and free radicals upon irradiation with UV–visible or near-infrared (NIR) light can easily degrade the harmful pollutant on to the glass surface [24]. Over the years, most common photocatalysts that are used to degrade organic pollutants are TiO_2 [25,26] ZnO [27] CdS [28] and Bi_2WO_6 [29]. Among these photocatalysts, TNPs are widely used for self-cleaning purpose due to their cost-effectiveness and strong photocatalytic property that can decompose dye pollutants such as Methylene Blue (MB), Methyl Orange (MO), Ethyl Violet and some other air pollutants [17].

It is established that TNPs possess high oxidative power, strong photo-stability, non-toxicity and antibacterial efficacy [1,17,30–34]. Furthermore, the empty d-shell of Ti^{4+} ions contributes to the large linear and nonlinear optical indices when incorporated inside glasses, indicating a very high oxygen hyperpolarizability of Ti−O pairs and large oxide ion electronic polarizabilities [35]. These are beneficial for broad array of technological purposes including biomaterials, photonic devices, semiconductors, and ionic conductors [36]. TNPs become super-hydrophilic under UV exposure, where a notable reduction in the WCA allows the formation of uniform water film on the surface and thereby prevents the deposition of the dirt above the surface layer [30]. Meanwhile, addition of sodium oxide (Na_2O) into glass help to increase the solubility of rare earth ions, which in turn improves the luminescence quantum yield of the glass [37,38] and enhances the electron excitation in TNPs with better photocatalytic action. Yet again, zinc oxide (ZnO) is an attractive compound that exhibits good photocatalytic activity, non-toxicity, superior chemical and thermal stability, good electrical and optical properties. It widely exploited for solar light activated photocatalysis, optoelectronic devices and sensor [33,39]. On the top, trivalent erbium ions (Er^{3+}) in erbium oxide (Er_2O_3) offer sharp up-conversion photoluminescence (PL) emission [40] in the visible region when doped inside glass [39], extend the absorption edge and provide extra photons beneficial for photocatalytic activity [39–41].

Currently, tellurite host based glass systems are greatly preferred because of their low phonon energy cut-off (600–700 cm^{-1}) that suppresses the non-radiative decay and provides optimum emission cross-section over the entire wavelength range [21]. Renewed interests towards the development of functional glass with synergism involving PL and self-cleanliness has resulted in valued materials as unconventional end-products [22]. Thus, embedment of self-cleaning photocatalytic agent (TNPs) into luminescent material (Er^{3+}-doped zinc tellurite glass) appear to be a synergistic strategy to customize the multi-functionality of binary/ternary inorganic glass system. However, a detail assessment of such synergism (self-cleanliness plus up-conversion luminescence) to realize tellurite glass system as prospective photoactive self-cleaning candidate is still lacking. Even though previous studies claimed that improved photocatalytic activity of glass can be achieved via the combined effects of Er^{3+} ions and TNPs by controlling the incoming photon [40,41], but a possible relationship between spectral and self-cleaning attributes of glass system is far from being developed. Specifically, the relation among WCA (wettability) and spectral (absorption and up-conversion emission) features of Er^{3+} ions doped tellurite glass embedded with TNPs is not clarified so far.

For the first time, we report the self-cleaning performance of Er^{3+} − doped (fixed contents of 1 mol%) tellurite glass system containing different TNPs concentration (varied from 0 to 0.4 mol%) in terms of WCA and degradation of MB [22]. The doping concentration of Er^{3+} is optimized by avoiding luminescence quenching [42]. Lower doping levels of Er^{3+} were maintained to avoid undesirable attenuations such as dipolar interactions and luminescence quenching [43]. Emission of Er^{3+} ion inside the sodium zinc-tellurite glass displayed optimum luminescence enhancement at 1.0 mol% of Er^{3+} doping before the luminescence quenching was likely to occur [44].Melt-quenching method is used to prepare Er^{3+}-doped tellurite glass with photocatalytic TNPs embedment. It is demonstrated that the present strategy of achieving hydrophilic self-cleaning glass is entirely different from conventional coating technique and is useful for practical outdoor applications [45]. A correlation between spectral modification and self-cleaning attribute of the proposed glass system is established. This approach may open up new avenues to fabricate multi-functional glasses with self-cleaning, anti-bacterial, energy conversion, and enhanced spectroscopic properties those are advantageous for sundry applications including buildings [46], solar modules [47] and optical devices [35].

2. Experimental procedures

2.1. Glass preparation

Series of glass samples with composition of (69-x)TeO_2-20ZnO-10Na_2O-1Er_2O_3-(x)TiO_2, where x = 0.0, 0.1, 0.2, 0.3 and 0.4 mol% were synthesized using the conventional melt quenching method. Table 1 summarizes the nominal compositions of the proposed glass system and their codes. About 15 g batch of analytical grade raw materials (powdered form) mixture (from Sigma Aldrich) including TeO_2 (purity 99.5%), ZnO (purity 99.9%), Na_2O (purity 80.0%), Er_2O_3 (purity 99.9%) and TNPs (purity 99.7%, anatase phase, size below 25 nm) were used as glass constituents and thoroughly ground. Then,

Table 1
Nominal compositions of the proposed glass system with respective codes.

Glass code	Glass composition (mol%)				
	TeO_2	ZnO	Na_2O	Er_2O_3	TNPs
TZNE	69	20	10	1	0
TZNE0.1Ti	68.9	20	10	1	0.1
TZNE0.2Ti	68.8	20	10	1	0.2
TZNE0.3Ti	68.7	20	10	1	0.3
TZNE0.4Ti	68.6	20	10	1	0.4
TZN	70	20	10	0	0
TZN0.4Ti	69.6	20	10	0	0.4

the mixture was melted in platinum crucible at 900 °C for 20 min in an electrical furnace. Subsequently, the melt was transferred to an annealing furnace and poured on the pre-heated stainless steel mould before being annealed at 300 °C for 3 h to reduce the presence of mechanical stress that could cause any embrittlement. Next, the solid samples were cooled down to room temperature. Finally, the solid samples were cut into desired dimension and polished to attain good transparency for further optical measurements.

2.2. Characterizations of glass samples

The amorphous nature of the as-prepared glass samples were examined using a MiniFlex300 X-ray Diffractometer (Rigaku, Japan) with Cu Kα radiations (λ = 1.54 Å), which was operated at 30 kV and 10 mA in the scanning angle (2θ) range of 20° to 80°. To detect the existence of TNPs inside the amorphous matrix transmission electron microscopic (TEM) imaging was carried out on a Hitachi H800 TEM operated at 200 kV. Thermal properties of the prepared glass were determined using a Perkin-Elmer differential scanning calorimeter (DSC) in the range of 200 °C to 500° C at a heating rate of 10 °C/min under N_2 gas atmosphere. The difference (ΔT) between the glass transition temperature (T_g) and the onset of crystallization temperature (T_x) was calculated, which roughly indicated a strong anti-crystallization. However, to evaluate accurately the resistance towards crystallization after the formation of glass, the parameter S for all the prepared glass was calculated following the Saad and Poulain relation given by [48]:

$$S = \frac{\Delta T \times (T_p - Tx)}{T_g} \tag{1}$$

where T_p is the peak crystallization temperature. Glass densities were determined by Archimedes method (Analytical balance with specific density-Precisa XT 220 A). Density (ρ) of glass samples were estimated via:

$$\rho = \rho_w \frac{Wa}{Wa - Ww} \tag{2}$$

where ρ_w is the density of distilled water (0.9975 g.cm^{-3}); W_a and W_w are the weight of the sample in the air and in the water, respectively.

The non-hydroscopic nature of tellurite glass does not induce any chemical reaction that affects the overall measurements. Therefore, use of water is more convenient, simple and economic than other immersing liquid media. The molar volume (V_m) of the glass samples were calculated using:

$$V_m = \sum_i \frac{x_i M_i}{\rho} \tag{3}$$

where x_i and M_i denote the molar fraction and molecular weight of the respective component. The refractive index (n) of the glass system were calculated using Dimitrov and Sakka relation [49]:

$$\frac{n^2 - 1}{n^2 + 2} = 1 - \sqrt{\frac{E_{opt}}{20}} \tag{4}$$

where E_{opt} is the optical band gap energy of the glass obtained from the UV absorption edge. The molar refractivity (R_m) yields:

$$R_m = \frac{n^2 - 1}{n^2 + 2}(V_m) \tag{5}$$

The glass polarizability (α_e) in terms of n was calculated using Lorentz-Lorenz relation of the from [50]:

$$\alpha_e = \frac{3}{4\pi}\left(\frac{R_m}{N_a}\right) \tag{6}$$

where N_a is the Avogadro's number.

The room temperature UV–Vis-NIR absorption spectra of all glass samples in the wavelength range of 400–1600 nm were recorded on a Shimadzu UV-3600PC scanning spectrophotometer (Kyoto, Japan). The absorption spectral data were further used to estimate the optical band gap energies associated with the direct and indirect transitions, Urbach energies, and refractive indices of the samples. The photon energy ($E = h\upsilon = hc/\lambda$) dependent optical absorption coefficient ($\alpha(\lambda)$) of the glass sample in terms of its thickness (y) and absorbance (A) or optical density was calculated via:

$$\alpha(\lambda) = \frac{2.303A}{y} \tag{7}$$

The optical band gap energy of the glass for both direct and indirect allowed transitions were evaluated using Davis and Mott theory [51]. In both transitions, the electromagnetic waves interact with the electrons in the valence band and raise them across the fundamental gap to reach the conduction band. The optical band gap was estimated via:

$$\alpha(\omega) = \frac{B(\hbar\omega - E_{opt})^r}{\hbar\omega} \tag{8}$$

where $B$is a constant, $\alpha(\omega)$ is the absorption coefficient at an angular frequency $\omega = 2\pi\upsilon$, $\hbar$ is the Planck constant divided by 2π and $r$is the index which can take on values of 1/2 and 2 corresponding to the direct allowed and indirect allowed transitions, respectively. Value of r is decided by the nature of electronic transitions responsible for the absorption process. Tauc's plots of $(\alpha\hbar\omega)^{1/r}$versus $\hbar\omega$ were generated to yield the value of direct and indirect optical band gap energy by extrapolating to the baseline at $(\alpha\hbar\omega)^2 = 0$ and $(\alpha\hbar\omega)^{1/2} = 0$, respectively. Urbach energy (ΔE) being the measure of the disordered nature of glassy phase was computed using the empirical relation:

$$\alpha(\omega) = B\exp\left(\frac{\hbar\omega}{\Delta E}\right) \tag{9}$$

where B is the band tailing parameter and ΔE is the width of the band tails of electron states called Urbach energy [42]. The value of ΔE was calculated from the reciprocal of the slope of the linear region of ln(α) versus $\hbar\omega$ plot [42]. The luminescence spectra were captured by a Hitachi F850 Fluorescence spectrometer (Tokyo, Japan), wherein a pulsed Xenon lamp was operated as excitation source. The emitted light was dispersed by Monk-Gillieson monochromators and subsequently detected using the standard photomultiplier tube. The slit widths of used monochromators were set at 10 nm for excitation and at 10 nm for emission with a scanning speed of 60 nm.min^{-1}. The emitted light was dispersed by Monk-Gillieson monochromators and detected using the standard photomultiplier tube. The Raman measurement in the wavenumber range of 200–1200 cm^{-1} was performed using a LabRAM HR-800 Horiba spectrophotometer (Kyoto, Japan) with excitation wavelength of 500 nm.

The wettability of the proposed glass system was determined using the sessile-drop method, wherein the WCA was measured by placing a water droplet on the glass surface exposed to air at ambient temperature. In this method, the water droplet was injected on the surface of the glass using 1 μL micro-pipette and the image of droplet on the glass surface was captured using a digital camera (Canon IXUS105) at fixed position. From the captured image, the WCA was estimated using the half-angle eq. [52,53]:

$$\theta = 2\tan^{-1}(h/d) \tag{10}$$

where θ is the WCA, h is the height of the water droplet (rested on glass surface) measured from centre of water baseline to the vertex of the water droplet and $2d$ is the distance across the baseline obtained by connecting the left end point to the right one. The surface tension of liquid (water) can be written in terms of the work of adhesion (W_A) between the water and glass interface using Young–Dupré eq. [54–57]:

$$W_A = \gamma_L(1 + \cos\theta) \tag{11}$$

where γ_L is the surface tension of the liquid (water). The surface

tension of water at room temperature (25 °C) was estimated to be ≈ 0.073 $N.m^{-1}$ [56]. Eq. (10) clearly shows that the material with low WCA (hydrophilic characteristic) have high interfacial solid-liquid surface tension [58]. This condition creates well-spread water film that wash out the dust from the glass surface under gravity when applied outdoor [59].

The photocatalysis performance of the samples was evaluated in terms of decomposition rate of MB in an aqueous solution under ultraviolet (UV) irradiation. Conventionally, MB dye is widely used to represent wastewater contamination. Thus, we selected it as the probe molecule for photodegradation rate determination [60]. In a typical process, first an aqueous solution of 5 ppm MB dyes and 0.01 g of photocatalyst glass sample (crushed in the form of powder) were magnetically stirred in darkness for 1 h to establish adsorption–desorption equilibrium. Then, the mixed specimen was placed in a 5 mL Petri dish and exposed to the UV irradiation (under a xenon lamp) of wavelength 350 nm and intensity 1 $mW.cm^{-2}$. The distance between the Petri disc bottom and light source was kept fixed ≈ 5.0 cm. The concentration of MB in the aqueous solution was analyzed by the UV–Vis absorption spectrometer (Shimadzu UV-2600, Kyoto, Japan) at constant time intervals of 2, 4, 6 and 8 min. The photodegradation behaviour of MB in the presence of the photocatalyst glass material was assumed to obey the first-order reaction kinetics given by:

$$\ln(C/C_0) = -kt \quad (12)$$

where k (min^{-1}) is the pseudo-first-order rate constant, t (min) is the irradiation time, C_0 and C are the initial and final (after time t) concentration of MB, respectively. Meanwhile, the half-life ($t_{1/2}$) of the chemical reaction was calculated following:

$$t_{1/2} = \ln 2/k \quad (13)$$

3. Results and discussion

3.1. XRD pattern

Fig. 1 shows the typical XRD pattern of prepared samples. Complete absence of any sharp peak and the presence of a broad hump in angular range of 20–30° in the diffractogram indicated the lack of crystalline order, thereby confirmed the true amorphous nature of the synthesized glass samples [61]. The sharp peaks from the TNPs nanocrystallites were not detected in this large angle XRD set up due to their extremely low contents in the host glass matrix. To detect the nanocrystalline peaks of TNPs small angle XRD is needed. Moreover, TEM imaging due to their high sensitivity could detect the nucleation of TNPs in specific-local area of the glass matrix [62,63].

3.2. Thermal characteristic

A glass with anti-crystallization is advantageous to maintain its properties during fiber drawing or any process that requires re-heating

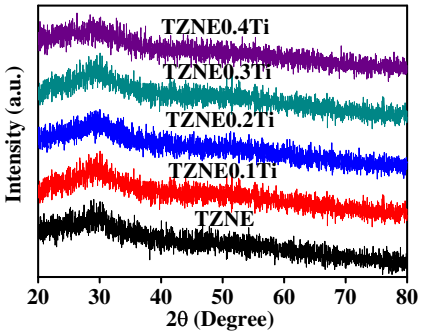

Fig. 1. Typical XRD patterns of proposed glass samples.

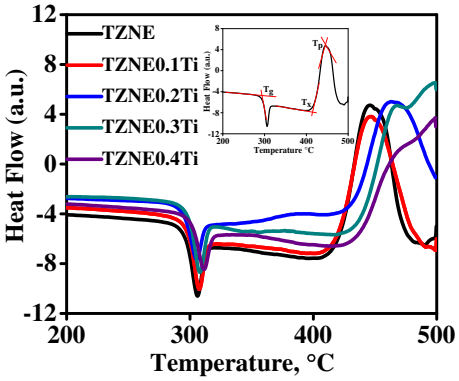

Fig. 2. Typical DSC curves of prepared glasses (inset: illustrating various characteristic temperatures of glass formation).

or re-melting of the glass for diverse applications. Their resistance over crystallization and heat are usually indicated by the thermal stability, where differential scanning calorimeter (DSC) is commonly used to obtain the characteristic temperatures (T_g, T_x, and T_p) [64]. A large difference between T_g and T_x ΔT roughly signifies the possession of strong anti-crystallization, where a value of ΔT above 100°C meet the requirement of conventional fiber drawing process [65]. Fig. 2 shows the DSC (Netzsch) curves of the prepared glass samples. The value of T_g, T_x and T_p were identified at the baseline inflexion in the DSC curves which were related to the heat capacity change between the glassy and viscoelastic phase [66]. Results in Table 2 depicts the TNPs contents dependent changes in the T_g (293–299 °C) and ΔT (121–138 °C) values for the studied glasses. The observed increase in the values of T_g and ΔT clearly indicated an enhancement in the thermal stability and delayed of crystallization process [66–68]. Besides, an increase in the S parameter value in the range of 13 to 17 °C with the increase of TNPs content reflected the large working range of fiber drawing ability and making other devices. This result is consistent with other reports [65,69].

3.3. TEM images

Figs. 3a and 3b show the TEM images for TZNE0.2Ti and TZNE0.4Ti glass, respectively with corresponding selected area of (646 nm × 485 nm) and (833.94 nm × 625.45 nm). The selected area is believed to be adequate to predict the mean TNPs size inside the glass network. Selected area for sample TZNE0.2Ti was smaller due to the low concentration of NPs, which was hardly traceable at lower magnification. Based on histogram of TNPs distribution fitted to the statistical LogNormal, Weibull and Gamma function, the estimated mean size of TNPs for TZNE0.2Ti and TZNE0.4Ti glass was 7 and 14 nm, respectively. The appearance of TNPs lattice spacing for sample TZNE0.4Ti is shown in Fig. 3c, which confirmed existence of TNPs inside the sample. The estimated lattice spacing of crystalline TNPs ≈ 0.36 nm. This lattice corresponded to the (101) face of anatase TNPs that matched with JCPDS card no. 21–1272 [70]. The observed wide range of TNPs distribution in the TEM image was attributed to mechanism of coalescence in which small NPs moved randomly via the Ostwald-ripening and transformed to a bigger size [71]. Coalescence process was emerged due to the availability of sufficiently high temperature during melting. Actually, the presence of high temperature could reduce the chances of agglomeration by providing great thermal energy to the small particles that underwent through surface diffusion and assembled via free energy minimization [62,72]. Consequently, bigger TNPs with diverse sizes were formed during glass synthesis which was decided by the high thermal energy mediated Brownian randomness, nucleation and growth mechanism [73].

Table 2
NPs concentration dependent variation in the thermal parameter of prepared glass system.

Sample	T_g, ± 1°C	T_x, ± 1°C	T_p, ± 1°C	ΔT, ± 1°C	S, ± 1°C	Ref.
TZNE	293	414	446	121	13	Present
TZNE0.1Ti	294	416	449	122	14	Present
TZNE0.2Ti	295	429	462	134	15	Present
TZNE0.3Ti	296	433	467	137	16	Present
TZNE0.4Ti	299	437	473	138	17	Present
$64TeO_2$-15ZnO-20CdO–$1V_2O_5$	333	468	485	135	7	[68]
$69TeO_2$-20ZnO-$5Na_2CO_3$-$5GeO_2$-$1Er_2O_3$	335	476	503	141	3	[69]

3.4. Physical properties

Tables 3 and 4 enlists the TNPs concentration dependent physical properties. The density of the prepared sample was decreased from 5.169–4.469 g·cm^{-3} with the increase of TNPs contents. This decrease in the density was due to the replacement of higher molecular weight (159.60 g·mol^{-1}) TeO_2 compound with lower molecular weight (79.876 g·mol^{-1}) TNPs. Meanwhile, the increase in the molar volume from 26.394 to 30.456 cm^3·mol^{-1} signified the creation of free volume by the embedded TNPs. The incorporation of TNPs generated more voids in the glass network, thus reduced the glass compactness as reported elsewhere [74]. Refractive index [75] and electronic polarizability [76,77] of the proposed glass system were also influenced by the embedment of TNPs in the host matrix. Refractive index of the glass was increased from 2.381 to 2.425 and the electronic polarizability was enhanced from 6.287 to 7.379 × 10^{-23} cm^3 with the increase of TNPs contents inside the glass. This increase of glass polarizability was ascribed to the reorganization of the tellurite glass network structure where large number of non bridging oxygen (NBO) ions were generated due to the formation of TeO_3 and TeO_{3+1} units. It is known that these NBOs have higher polarizability than BOs in the TeO_4 units [78,79]. This result was agreed with the report of Azlan et al. (2015) which claimed a linear relationship between the electronic polarizability and the refractive index [80].

Indirect and direct band gap energies were decreased with the increase of TNPs contents and ranged between 3.059 and 2.898 eV and 3.076 to 3.030 eV, respectively [51]. Observed narrowing in the optical band gap energies were attributed to lowering of average bond energy due to formation of more NBO than BO in the glass network [43,81]. Recently, Ismail et al. (2016) demonstrated the reduction in the optical band gap with the addition TNPs which was attributed to the generation of higher number of NBO than BO ions in the glass host [82]. Actually, the presence of large number of NBOs implies the abundance of localized electrons which may act as donor centre in the glass network. Occurrences of these donor centres in turn could shift the absorption edge towards higher wavelength (lower energy) and enabled the electron uplifting from the valence band to the conduction band [82]. Furthermore, the increase in Urbach energy (0.307–0.846 eV) with increasing TNPs contents indicated an enhanced disordering in the glass network, implying more extension of the localized states within the optical band gap. These ΔE values were calculated from inverse slope of ln(α) versus $\hbar\omega$ plot as shown in Fig. 4 [83]. It is established that glass system with large Urbach energy has higher tendency to convert weak bonds into defects [84] which is agreed with the previous finding [28].

3.5. Water contact angle (WCA) and surface tension (ST)

Control of the glass wettability is the key factor to achieve the self-cleaning attributes [18]. Glass with high hydrophilicity (high wettability or low WCA) allows the water to spread onto the surface which can roll or sweep the pollutant particles easily, result in self-cleaning effect [85]. The wettability characteristic of the glass surface can be quantified by estimating its WCA which is related to the glass ST. The lowering of the WCA of the glass surface implies an increase in the wettability and vice versa [59]. Table 5 compares the measured WCA of the present Er^{3+}-doped tellurite glass without and with containing TNPs with other reported glass system in the literature. Fig. 5 illustrates the variation WCA of the glass system as a function of TNPs contents. The inserted photographs on the WCA angle measurement procedure clearly revealed the reduction of CA from 68.0° to 43.0° with the increase of TNPs contents from 0.0 to 0.4 mol%. This observed shrinking in the WCA was assigned to the enhancement of glass surface hydrophilicity. For hydrophilic surface, the adhesive forces (attractive forces between water molecule and surface of the glass) are stronger than the cohesive forces (attractive forces between water molecules). In the present case, the calculated value of the work of adhesion (ST) was varied in the range of 0.100–0.126 Nm^{-1} (Table 5) when the TNPs content was increased from 0.0 to 0.4 mol%. The achievement of high adhesion in the prepared glass system could allow the spreading of water across the glass surface which was certainly advantageous for sweeping (washing away) the deposited pollutant particles.

According to Sonder et al. (1950), the force exerted on the surface depends on the structural and chemical composition of the host glass [86]. Interestingly, host glass containing hyper polarizable ions such as TNPs [35] can modify the force field that acts upon the glass surface. This in turn can alter the electron distribution on the glass surface and induces asymmetric force field that exists between neutral metal atom

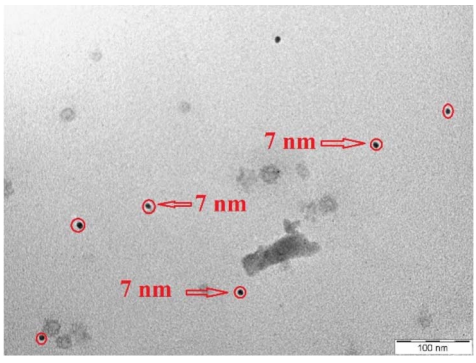

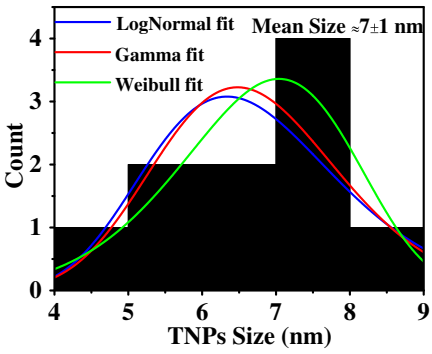

Fig. 3a. TEM image of TZNE0.2Ti glass together with TNPs histogram distribution.

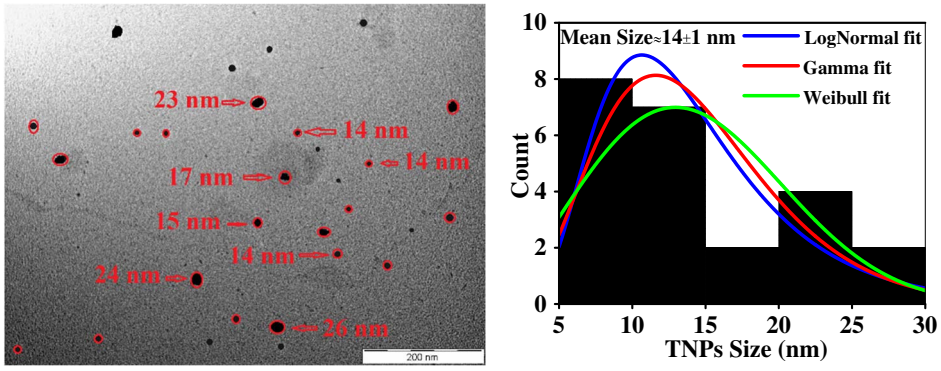

Fig. 3b. TEM image of TZNE0.4Ti sample with respective TNPs histrogram distribution.

and the negatively charged oxygen ions (O^{2-}). This asymmetric force exerts strong ionic interaction towards the oxygen ions at one interfacial side but remains natural at the opposite side. Consequently, incoming water molecules faces higher tendency of attraction and chemisorption at the glass surface. Briefly, glass surface containing strong polarizable ions such as TNPs can influence the surface tension, hygroscopicity, catalytic properties, as well as adhesion forces on the glass surface [86]. Thus, such surfaces become more hydrophilic in the order of: non-polar < polar, no hydrogen-bonding < polar, hydrogen-bonding < hydroxylic < ionic. This shows that the structure and physical properties (refractive index, density, electronic polarizabilities) of the glass containing TNPs have significant influence on the wettability [87].

Understanding the behaviour of water droplets on diverse glass surfaces is important to achieve the optimum composition for designing glass with self-cleaning operation [90]. Currently, self-cleaning materials operate under two principles namely hydrophobicity and hydrophilicity [91]. However, the other principal mechanism of inducing the self-cleaning effect in glass which is considered to be the best one yet remains unknown. Furthermore, existing literature seldom clarified the influence of TNPs or AgCl NPs photocatalyst incorporation on the wettability and self-cleanliness mechanisms of the glass system. Therefore, WCA of the present glass system was compared with the previous findings involving the the glass wettability control from hydrophobic to hydrophilic character. In such cases, the modification of the glass chemical composition played a significant role and revealed some implications towards the need of fundamental research and feasibility of practical technological applications [92].

It was reported that the WCA in Er^{3+}/Nd^{3+}-doped lithium niobate tellurite glass system (coded as TLNENA*x*) was increased from 25.5° to 47.4° with the increase of AgCl NPs contents [88]. Ismail et al. (2016) also claimed an increment in the WCA from 63.1° to 71.0° for zinc-magnesium phosphate glass (named as PZMTi*x*) doped with varying concentrations of TNPs (range $1.0 \leq \times \leq 4.0$ mol%) [89]. These studies emphasized that the hydrophilic nature of the glass can be controlled by adjusting the concentrations of TNPs. Theoretically, wettability characteristics of the glass can be tuned by altering the ST [93,94]. Generally, phosphate glass possesses strong hydrophilicity and high surface tension ($\approx 0.25\ Nm^{-1}$) [94–97] compare to tellurite glass ($\approx 0.16\ Nm^{-1}$) [94]. The polar characteristics of phosphate glass system are decided by the occurrence of negative charge on the phosphate group (polar head). This polar head can strongly attach the water molecules from their surroundings. Although TNPs are super-hydrophilic in character with surface tension of $1.95\ Nm^{-1}$ [98], however previous study displayed that the surface energy of phosphate glass system gets reduced due incorporation of TNPs at different contents [96]. The observed decrease in the glass surface energy was ascribed to the formation of more thermally stable hydration-resistant Ti-O-P bonds by replacing the hydration-susceptible P-O-P bonds [89,97].

For tellurite system, the glass-water interfacial surface tension is enhanced with the increase of TNPs embedment at low concentration, which in turn augmented the hydrophilic nature of the glass. Nurhafizah et al. (2016) reported a significant drop in the Raman intensity of tellurite glass system due to the inclusion of AgCl NPs in the concentration range of 1.0–3.0 mol%, which was ascribed to the reduction of polarization within the glass system [88]. Although the surface energy of AgCl NPs is almost comparable with TNPs ($1.12\ Nm^{-1}$) [98], but the observed enhancement in the glass wettability with increasing AgCl NPs content was majorly attributed to the augmentation of the WCA due to reduced polarization effects. In short, we demonstrated that Er^{3+}-doped tellurite glass with hydrophilic character (WCA below 90°) can be achieved by embedding TNPs at different concentrations [88]. Furthermore, the observed reduction in the WCA was attributed to the photocatalytic TNPs induced super-hydrophilic effect in the glass system. This super-hydrophilic effect allowed the formation of a uniform water film on the glass surface which in turn could prevent the deposition of dirt particles on the surface and promoted self-cleanliness [31,85].

3.6. Photocatalytic action

Fig. 6 shows adsorption spectra of MB solution containing Er^{3+} ion

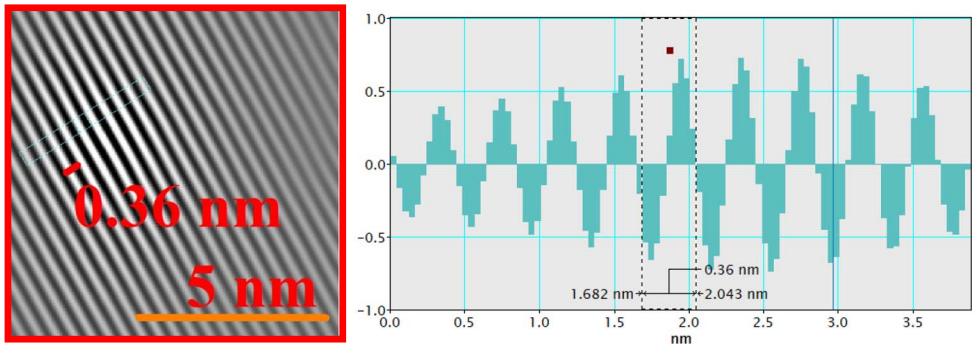

Fig. 3c. HRTEM image of TNPs and the lattice fringe profile revealing the spacing.

Table 3
TNPs content dependent average values of molecular weight, refractive indices, density, molar volume and polarizability of the glass system.

Glass code	M_v (± 0.01 g·mol^{-1})	n	ρ (g·cm^{-3})	V_M (cm^3·mol^{-1})	α_e(× 10^{-23} cm^3)
TZNE	136.43	2.38 ± 0.01	5.17 ± 0.22	26.39 ± 1.13	6.29 ± 0.27
TZNE0.1Ti	136.35	2.40 ± 0.01	4.86 ± 0.20	28.06 ± 1.16	6.73 ± 0.28
TZNE0.2Ti	136.27	2.40 ± 0.02	4.65 ± 0.22	29.31 ± 1.36	7.03 ± 0.33
TZNE0.3Ti	136.19	2.40 ± 0.02	4.54 ± 0.19	30.00 ± 1.26	7.21 ± 0.31
TZNE0.4Ti	136.11	2.43 ± 0.01	4.47 ± 0.15	30.46 ± 1.05	7.38 ± 0.26

Table 4
TNPs content dependent values of direct band gap, indirect band gap and Urbach energy.

Glass code	E_{dir} (± 0.01 eV)	E_{indir} (± 0.01 eV)	ΔE (± 0.01 eV)
TZNE	3.08	3.06	0.31
TZNE0.1Ti	3.07	3.00	0.34
TZNE0.2Ti	3.06	2.99	0.37
TZNE0.3Ti	3.05	2.98	0.52
TZNE0.4Ti	3.03	2.90	0.85

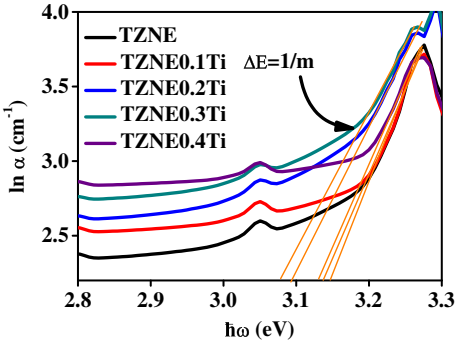

Fig. 4. Plot of ln(α) against photon energy for estimating the Urbach energy of glass system with different NPs contents.

glass with different TNPs amounts after 8 min irradiation. Reduction of MB adsorption at 664.5 nm is seen with addition TNPs. Meanwhile Table 6 enlists the values of the kinetic rate constant (k) and half-life ($t_{1/2}$) of the reaction. Fig. 7 shows the TNPs concentration dependent rate constant (k), where sample containing 0.2 mol% TNPs revealed optimum value of k. The value of k is obtained from the slope of linear fitting ln(α) against irradiation time for each glass sample as depicted in the inset. The achievement of higher k value indicated faster degradation of MB, signifying a better photocatalytic action by the glass.

Actually, the presence of Er^{3+} ions played a vital role in enhancing the photocatalytic activity of TNPs through interfacial charge transfer and effective prevention of electron-hole pairs [40]. Sample with 0.1 mol% of TNPs (high ratio of Er^{3+} ion to TNPs) revealed a narrowing in the bandgap and generated large number of photo-induced electron-hole pair. However, sample with too narrow bandgap led to the recombination of electron-hole pairs and thus reduced the reaction kinetic rate responsible for the MB degradation [99]. The appearance of imbalanced ratio of Er^{3+} to TNPs distorted the charge-separation

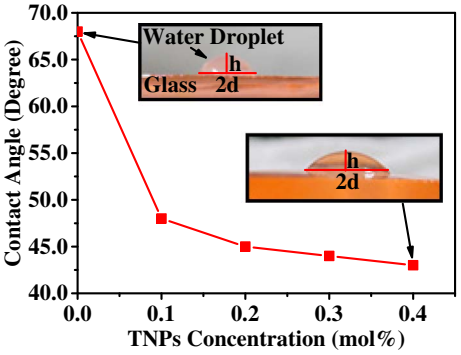

Fig. 5. TNPs concentration dependent variation of the WCA for the glass system.

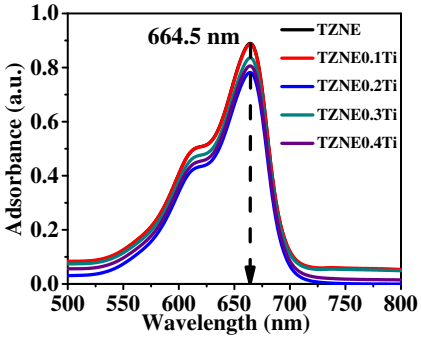

Fig. 6. Adsorption spectra of MB solution after 8 min of irradiation for the studied glasses with different TNPs contents.

Table 6
TNPs content dependent pseudo first-order rate constant and half-life of MB degradation.

Glass code	TNPs content (mol%)	k (min^{-1})	$t_{1/2}$ (min)
TZNE	0	0.01820	38.0850
TZNE0.1Ti	0.1	0.01693	40.9420
TZNE0.2Ti	0.2	0.01979	35.0251
TZNE0.3Ti	0.3	0.01001	69.2455
TZNE0.4Ti	0.4	0.00785	88.2990

Table 5
Comparison of the measured WCA and ST for the present glass system with other reports.

Glass code	Type of NPs used	Metal NPs contents (mol%)	WCA (± 0.1°)	ST (± 0.001 N.m^{-1})	Reference
TZNE	–	0.0	68.0	0.100	Present
TZNE0.1Ti	TiO_2	0.1	47.0	0.123	Present
TZNE0.2Ti	TiO_2	0.2	45.0	0.125	Present
TZNE0.3Ti	TiO_2	0.3	44.0	0.125	Present
TZNE0.4Ti	TiO_2	0.4	43.0	0.126	Present
TLNENA*x*	AgCl	3.0	47.4	–	[88]
PZMTi*x*	TiO_2	4.0	71.0	–	[89]

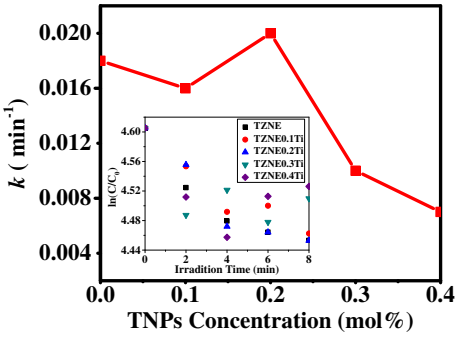

Fig. 7. TNPs concentration dependent rate constant (k) (inset: plot of $\ln(C/C_0)$ versus irradiation time).

efficiency for photocatalytic action via electron transfer [100]. As the TNPs concentration was increased, an efficient separation between Er^{3+} and TNPs could promote more $^{\bullet}OH$ and $^{\bullet}OH^{-}$ radical for higher photocatalytic activity [40]. However, at higher TNPs concentration the NPs grew bigger via coalescence mechanism [101]. Consequently, the specific area of the active site for the photocatalytic action appeared less. The existence of strong empirical correlation between the surface area and NPs size suggested that for larger particle size the photocatalytic reaction rate was slowed down [102].

The k value of MB for glass sample containing 0.2 mol% TNPs was found to be higher than the one with 0.4 mol%, This observation was attributed to the effect of particles size that could alter the active site responsible for photocatalytic action [103,104]. The sample containing 0.2 mol% of TNPs (mean size of 7 nm) could degrade the MB better than the one with 0.4 mol% of TNPs (mean size 14 nm). This clearly displayed that smaller TNPs possessed better photocatalytic action than larger one. However, Kim et al. (2007) acknowledged that there is an optimum TNPs size that could play important role in MB degradation. In their study, TNPs with size 8 nm exhibited the optimum k in degrading MB, indicating the highest photocatalytic activity in the system. Moreover, TNPs with size above 10 nm and below 6 nm started to reveal a reduction in k value, which was ascribed to the alteration in the surface area, wherein TNPs crystallites and quantities of hydroxyl groups attached on the TNPs were responsible for the photocatalytic performance [105].

Conversely, the TNPs concentration dependent variation of $t_{1/2}$ showed the reverse trend than k. This increase of k and shortening of $t_{1/2}$ in the glass system signified the enhancement of photocatalytic activity. Moreover, it was found that the glass with highest TNPs concentration does not necessarily have utmost photocatalytic action, which could be due to the inefficient charge transfer within TNPs species or between TNPs and other ions inside the glass [106]. At higher concentration these NPs suffered partial aggregation [40,41] and formed two coordination states including Ti^{4+} or Ti^{3+} originated from the interfacial charge transfer during the melting process [107]. Presence of Ti^{3+} species associated with oxygen vacancies [25,108] enhances the absorption of visible light [109,110]. The availability of Ti^{3+} sites able to built-in donor energy level under the conduction band of TNPs and thereby diminishes the interfacial energy barrier between Er_2O_3 and TNPs. Therefore, the migration of electrons from Er_2O_3 to the conduction band of TNPs becomes feasible, which in turn promotes the separation of photo-generated charge carriers and reduces the combination rate. The Ti^{3+} species also narrows the bandgap of TNPs and trigger the visible-light activity of TNPs. Also, the generated holes of TNPs can transfer to the valance band of Er_2O_3, which support the charge separation [41,111]. In other word, coupling of Er_2O_3 and TNPs could be a potential pathway not only to extend the light absorption of TNPs to visible range via surface plasmon resonance (SPR), but also to strengthen the charge carriers transfer by forming heterojunction at the interface [111,112]. However, excess TNPs inside the glass may result in bigger particles following Ostwald ripening process [71]. Consequently, the Ti^{3+} concentration reduces and the recombination rate of the photo-produced carriers in TNPs is increased, declining the photocatalytic activity [113]. It is worth noting that high recombination rate of electron-hole pair could reduce the promotion of $^{\bullet}OH$and $^{\bullet}O^{-}$ radical that was responsible in oxidising the pollutants on the surface of the glass and break them down into simpler compounds such as carbon dioxide and water molecules [114,115]. The photocatalytic system typically can be represented via the following chemical reaction:

$$\text{Organic} + O_2 \xrightarrow{h\nu \geq E_{gap}(TNPs)} CO_2 + H_2O$$

where E_{gap} (≈ 3.2 eV) is the TNPs band gap, revealing the requirement of UV-light for the reaction to occur. Moreover, improved TNPs absorbance to visible light via creations of Ti^{3+} ions [116] and strong oxidation stability supported by Er^{3+} ions [111] are responsible for the increase of photocatalytic activity sites to degrade MB and vice versa [103].

Based on the present observation, it is established that interfacial charge transfer via multi-component system (TNPs and Er^{3+} ion) could inhibit the recombination of photogenerated charge carriers and thereby altered the photocatalytic activity of the glass [24]. Fig. 8 depicts the visible light absorption ability of Er^{3+} ions (up-conversion luminescence agent) and subsequent excitation TNPs to generate electron-hole pairs [117]. It was affirmed that the TNPs enabled efficient generation and separation of electron–hole pairs in the present glass system played a vital role towards the enhancement of photocatalytic activity [22]. Therefore, it was suggested that an optimum concentration of Er^{3+} ions and TNPs must be maintained to promote the effective charge transfer and subsequent increase in the available photocatalytic sites inside the glass, which is vital for long-term self-cleaning activity [59,103].

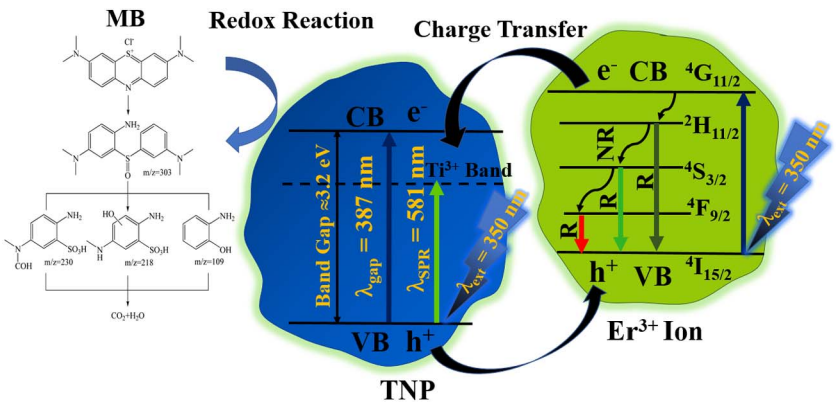

Fig. 8. Schematic diagram showing the photogeneration and separation of electron-hole pairs in TNPs.

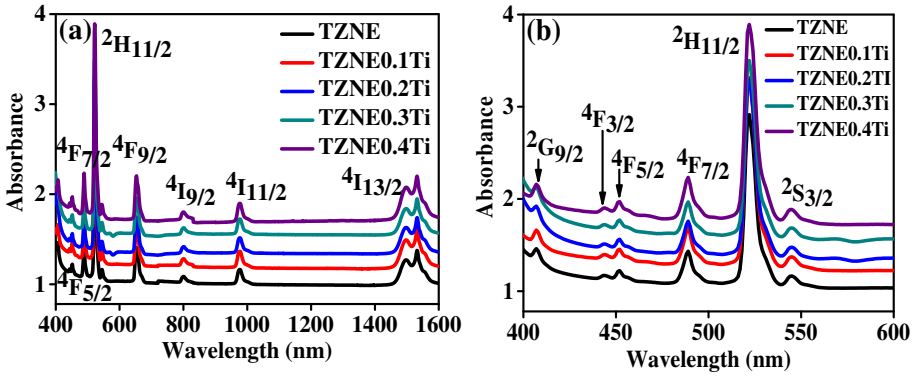

Fig. 9. Absorption spectra of all synthesis glass (a) in the range 400–1600 and (b) in the range 400–600 nm.

3.7. UV–vis-NIR absorption spectra

Fig. 9 (a) presents the typical UV–Vis-NIR absorption spectra of all samples in the wavelength range of 400–1600 nm. Meanwhile Fig. 9 (b) shows absorption spectra in shorter range which is 400–600 nm in order to observe the bands clearly. The absorption spectra comprised of ten absorption bands centred around 407, 444, 452, 489, 522, 552, 653, 800, 976 and 1532 nm which were assigned to the transition from the Er^{3+} ion ground state of $^4I_{15/2}$ to the excited states of $^2G_{9/2}$, $^4F_{3/2}$, $^4F_{5/2}$, $^4F_{7/2}$, $^2H_{11/2}$, $^4S_{3/2}$, $^4F_{9/2}$, $^4I_{9/2}$, $^4I_{11/2}$ and $^4I_{13/2}$, respectively [118]. The absorbance of the glass was enhanced with the increase of TNPs contents, which was attributed to the TNPs SPR mediated effects [119]. The SPR assisted electromagnetic field augmentation around the TNPs triggered strong electron excitations in the ground state of Er^{3+} ions and thereby enhanced the excited states transition probability and the absorbance [120]. This result was consistent with the previous findings [121]. Enhanced absorbance was advantageous for strong photocatalytic action of TNPs.

3.8. PL spectra

Fig. 10 illustrates the TNPs concentration dependent PL spectra of all glass samples under the excitation wavelength of 490 nm. The intensity and bandwidth of each spectrum was found to be sensitive to TNPs contents. Three prominent bands are evidenced centred around 535, 555 and 670 nm which were allocated to transitions of $^2H_{11/2} \rightarrow {}^4I_{15/2}$, $^4S_{3/2} \rightarrow {}^4I_{15/2}$ and $^4F_{9/2} \rightarrow {}^4I_{15/2}$, respectively. The inset of Fig. 10 shows the surface plasmon absorption band (centred at ≈ 581 nm) of TNPs for TZN0.4Ti glass sample devoid of Er^{3+} ions.

Table 7 summarizes the maximum enhancement factor of the emission band intensity for all prepared glass samples. Sample containing 0.2 mol% of TNPs displayed the maximum intensity enhancement by a factor of 6.77, 4.56 and 2.00 times corresponding to emission band centred at 535, 555 and 670 nm, respectively. The observed PL intensity enhancement was attributed to the effect of localized SPR mediated colossal electric field of TNPs in the proximity of Er^{3+} ions [42]. The PL enhancement factor were estimated by dividing the maximum intensity of each PL band (535, 555, 670 nm) for the glass samples with varying TNPs content (TZNE0.1Ti, TZNE0.2Ti, TZNE0.3Ti, TZNE0.4Ti) with the one without containing TNPs (TZNE). This SPR involved the manipulation of light on the nanoscale, where strong local electric field was generated originally from the collective electron oscillations of TNPs and subsequent coupling with the incoming laser radiation at the same frequency [43]. The PL intensity of the green bands (535 and 555 nm) showed highest enhancement due to their closeness to surface plasmon band (581 nm) [42]. However, further increase of TNP_S contents beyond 0.2 mol% inside the glass caused luminescence quenching. The occurrence of quenching was attributed to the mechanism of energy transfer (ET) from the excited Er^{3+} ions to the TNPs ($Er^{3+} \rightarrow$ Ti) in the form of thermal energy dissipation [42]. Furthermore, sample exhibiting highest PL enhancement also revealed strongest photocatalytic performance. It was asserted that Er^{3+} ions to TNPs concentration ratio of 1:0.2 is most favourable to achieve their efficient synergism in zinc-sodium tellurite glass system, which further could improve the spectral attributes and photocatalytic performance simultaneously.

Table 7
TNPs concentration dependent maximum enhancement factor of the prepared glass system.

Glass code	TNPs (mol%)	Enhancement factor 535 nm:555 nm:670 nm
TZNE	0	1: 1: 1
TZNE0.1Ti	0.1	3.23: 1.74: 1.93
TZNE0.2Ti	0.2	6.77: 4.56: 2.00
TZNE0.3Ti	0.3	1.87: 1.01: 1.40
TZNE0.4Ti	0.4	1.16: 1.09: 1.06

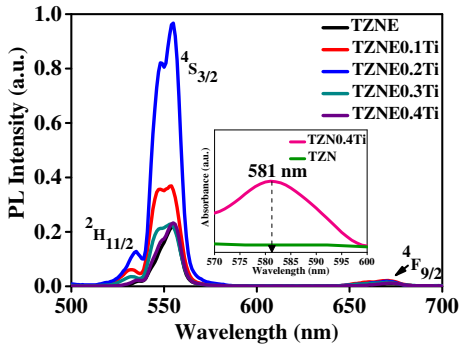

Fig. 10. TNPs concentration dependent room temperature PL spectra of all samples under the excitation wavelength of 490 nm (inset: SPR band of TNPs for TZN0.4Ti glass sample).

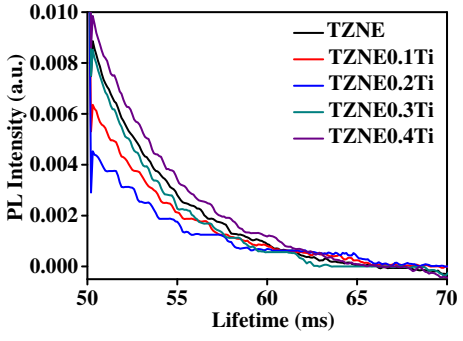

Fig. 11. Room temperature PL decay curves of Er^{3+} ($^4S_{3/2}$) inside the studied glasses.

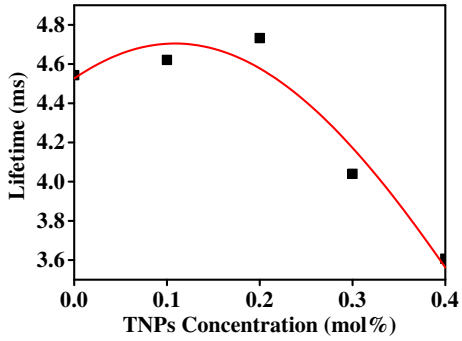

Fig. 12. TNPs concentration dependent variation in the PL lifetime of Er^{3+} ($^4S_{3/2}$ level) inside the synthesized tellurite glass.

3.9. Time-resolved PL decay

Fig. 11 shows the room temperature time-resolved PL decay profile of Er^{3+} ($^4S_{3/2}$ level) for the studied glasses without and with TNPs contents under the excitation wavelength of 490 nm. The measured lifetime ($\tau_{measured}$) is given by:

$$\tau_{measured} = \frac{1}{I_o}\int I(t_{PL})\, dt_{PL} \tag{13}$$

where $I(t_{PL})$ and I_o are the PL intensities at time t_{PL} and at $t_{PL} = 0$, respectively [122,123]. To simply the calculation, the experiment data is fitted with the following function:

$$I(t_{PL}) = I_o \exp\left(\frac{-t_{PL}}{\tau}\right) \tag{14}$$

where $\tau$is the decay time [124].

Fig. 12 illustrates the TNPs concentration dependent variation in the PL lifetime of Er^{3+} ($^4S_{3/2}$ state) doped inside the tellurite host. The PL lifetime was slightly increased at first from 4.5 to 4.7 ms and then dropped to 3.6 ms as the amount of TNPs was exceed beyond 0.2 mol%. This result is in good agreement with the measured steady-state PL spectra for the respective glass (Fig. 10). The observed elongation in the PL lifetime was ascribed to the enhanced local electric field effect and the energy transfer from the TNPs to Er^{3+} ($^4S_{3/2}$ level). Conversely, the shortening in the PL lifetime was attributed to the energy transfer from Er^{3+} to TNPs [122,125].

3.10. Raman spectra

Fig. 13 (a) displays the Raman spectra of the proposed glass system. Fig. 13 (b) shows the deconvoluted Raman spectrum of TZNE0.4Ti glass sample, which consisted of five vibrational bands positioned around the wavenumber of 388 (A), 495 (B), 673 (C), 758 (D), and 845 (E) cm^{-1}. Table 8 enlists the typical Raman band assignments for TZNE0.4Ti glass. Irrespective of TNPs contents, each spectrum revealed nearly similar pattern but different intensity. The vibration band indexed as A around 388 cm^{-1} was assigned to the Zn—O bond vibration [43,89]. This band and the band indexed as B around 495 cm^{-1} were assigned to the symmetrical stretching or bending vibrations of Te–O–Te linkages formed by sharing vertices of TeO_4, TeO_{3+1} and TeO_3 tp units [43]. The vibration band indexed as C around 673 cm^{-1} was allocated to the antisymmetric stretching of the continuous network Te-O-Te linkages composed of TeO_4 unit [43]. These linkages were characterized by long and short Te—O bonds. The difference in the polarizability between the long and short Te—O bonds may be responsible for the significant intesification of the Raman signal [43]. The vibration band around 758 cm^{-1} labeled as D was approved to the stretching modes of Te—O^- and Te=O bonds containing NBOs in TeO_{3+1} polyhedra and TeO_3 units [126,127]. Lastly, the vibration band at 845 cm^{-1} labeled as E was assigned to the stretching vibration of TeO_3 units which also contained NBOs. Moreover, vibration bands designated as D and E were not usually observed in pure tellurite glass [43]. Complete absence of any well-resolved Raman band corresponding to TNPs and Er^{3+} ions in the host glass was majorly attributed to their low concentrations and good dispersion in to the entire amorphous network without any agglomerations [88]. Actually, Zn—O bonding vibration are more favoured for glass transformation whereas Na—O bonding vibration tend to preserve the glass network [128]. Present results on Raman studies revealed nearly the same bonding vibration as reported in the literature [43].

Table 8
Raman peak shifts (in cm^{-1}) and band assignments of TZNE0.4Ti glass.

Band	Raman shift (cm^{-1})	Assignment of band	Reference
A	388	Zn-O bond vibration	[43,89]
B	495	Symmetric stretching or bending Te-O-Te vibration	[43]
C	673	Asymmetric stretching TeO_4 vibration	[126,127]
D	758	Stretching TeO_3/TeO_{3+1} vibration	[126]
E	845	Stretching isolated TeO_3 vibration	[129]

Fig. 14 shows the Raman intensity enhancement factor of the synthesized glass system. The enhancement factor were determined by dividing the maximum intensity of the de-convoluted band of sample containing TNPs with the one without TNPs inclusion (TZNE). Overall, the Raman intensity was enhanced with the increase in TNPs contents. TZNE0.4Ti sample revealed the maximum Raman intensity enhancement by a factor of 2.25, 1.83, 1.98, 1.56, 1.87 and 3.58 corresponding to the band centred around 388 (A), 495 (B), 673 (C), 758 (D), and 845 (E) cm^{-1}, respectively. Furthermore, the Raman band indexed as E exhibited the highest enhancement due to strong polarizability of TeO_3 units. This enhancement was attributed to the generation of more TeO_3 units due to the conversion of TeO_4 and TeO_{3+1} units with the addition TNPs [129]. TNPs mediated SPR effect played a significant role in the observed Raman intensity enhancement [43]. It worth noting that Raman intensity is linearly dependent on the local field enhancement and polarization [130].The mechanism of Raman intensity

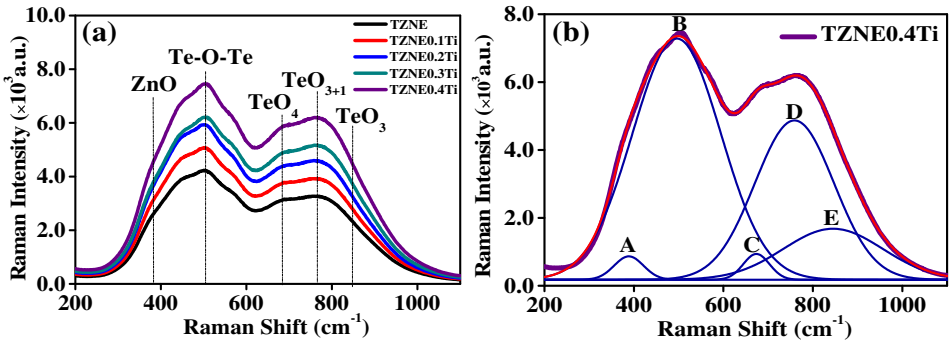

Fig. 13. (a) Raman spectra of all prepared glass samples and (b) de-convoluted Raman spectra of TZNE0.4Ti glass sample.

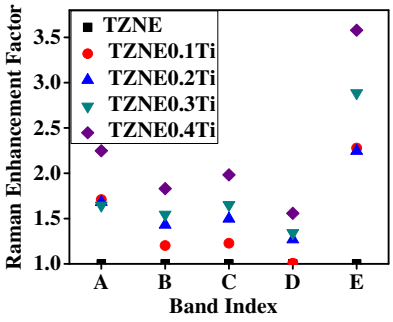

Fig. 14. Raman enhancement factor for all synthesis glass.

amplification by several orders of magnitude is called Surface Enhanced Raman Scattering (SERS) [131], which originates from the interaction of glass molecule with the metal NPs surface plasmon. It is affirmed that the local field enhancement induced by SPR effect together with the hyperpolarizability of TNPs were responsible for SERS phenomenon [89].The SERS evidenced in the present glass system is indeed correlated to the WCA (wettability) which is responsible for its self-cleanliness attributes as indicated in Fig. 5 [88,89].

Briefly, the ratio of Er^{3+} ion to TNPs concentration played a vital role, which led to an alteration in the spectral properties and induced self-cleaning action to the prepared glasses. In this work, incorporation of 0.2 mol% of TNPs in the glass showed the optimum enhancement in overall properties where the mean size of TNPs was 7 nm. The TNPs mediated SPR effect could modify the local electric field in the proximity of Er^{3+} ion and subsequently altered the absorbance as well as luminescence properties of Er^{3+} ions [101]. Raman enhancement confirmed the changes in polarizability that was induced by the TNPs assisted SPR effect. Besides, the size variation of TNPs could influence the wettability and photocatalytic performance of the glass. This observation was attributed to the alteration in the available oxygen vacancies which created enhanced hydrophilic surface and allowed photocatalytic degradation of organic pollutants by providing active sites. Consequently, it reduced the number of O_2 and led to the formation of superoxide radicals and hydroxyl radicals [132]. The intensified absorbance and luminescence of Er^{3+} ion could reduce the TNPs band gap and provide more electron to facilitate the pollutant degradation [132,133]. A correlation between the spectral and self-cleaning attributes of the glass system was established. This new knowledge may be significant in designing the multi-functional advanced material for solar module, optical devices and biomedical sensors [99,134].

4. Conclusion

A series of Er^{3+}-doped zinc tellurite glass with varying concentration of TNPs were prepared using melt-quenching technique. For the first time, the spectral and self-cleaning attributes of this glass system was determined as a function of TNPs concentration. TEM images manifested the nucleation of TNPs in the amorphous matrix. The WCA of the glass was reduced with the increase of TNPs contents, indicating their super hydrophilic character. Glass containing 0.2 mol% TNPs displayed highest photocatalytic activity towards MB photodegradation rate and PL intensity enhancement. The detection of SERS signal authenticated the presence strong polarizability and enlargement of SPR mediated local electric field due to the embedment of TNPs in the host glass, which in turn affected the glass wettability. A relationship between TNPs assisted modification in the spectral and self-cleaning properties was established. Present findings may be beneficial for the development of multi-functional self-cleaning glasses.

Acknowledgement

The authors gratefully acknowledge the financial support from UTM via Vot. GUP/RU 12H42, 13H50 and 17H19 and Malaysian Ministry of Education through FRGS 4F424 and 4F892. Nabihah is also grateful to Osaka University, Japan and Professor Norikazu Nishiyama for their limitless support and encouragement.

References

[1] X.T. Zhang, O. Sato, M. Taguchi, Y. Einaga, T. Murakami, A. Fujishima, Self-cleaning particle coating with antireflection properties, Chem. Mater. 17 (2005) 696–700, http://dx.doi.org/10.1021/cm0484201.
[2] H.K. Raut, V.A. Ganesh, A.S. Nair, S. Ramakrishna, Anti-reflective coatings: a critical, in-depth review, Energy Environ. Sci. 4 (2011) 3779, http://dx.doi.org/10.1039/c1ee01297e.
[3] P. Ragesh, V. Anand Ganesh, S.V. Nair, A.S. Nair, A review on "self-cleaning and multifunctional materials,"7, J. Mater. Chem. A 2 (2014) 14773–14797, http://dx.doi.org/10.1039/C4TA02542C.
[4] M. Zhang, S. Feng, L. Wang, Y. Zheng, Lotus effect in wetting and self-cleaning, Biotribology 5 (2016) 31–43, http://dx.doi.org/10.1016/j.biotri.2015.08.002.
[5] L. Yao, J. He, Recent progress in antireflection and self-cleaning technology – from surface engineering to functional surfaces, Prog. Mater. Sci. 61 (2014) 94–143, http://dx.doi.org/10.1016/j.pmatsci.2013.12.003.
[6] B. Huang, Y. Zhou, F. Yang, L. Wu, Y. Qi, J. Li, The 1.53 μm spectroscopic properties of $Er^{3+}/Ce^{3+}/Yb^{3+}$ tri-doped tellurite glasses containing silver nanoparticles, Opt. Mater. 51 (2016) 9–17, http://dx.doi.org/10.1016/j.optmat.2015.11.004.
[7] S. Yildirim, M. Yurddaskal, T. Dikici, I. Aritman, K. Ertekin, E. Celik, Structural and luminescence properties of undoped, Nd^{3+} and Er^{3+} doped TiO_2 nanoparticles synthesized by flame spray pyrolysis method, Ceram. Int. 42 (2016) 10579–10586, http://dx.doi.org/10.1016/j.ceramint.2016.03.131.
[8] A. Pandey, V. Kumar, R.E. Kroon, H.C. Swart, Photon upconversion in $Ho^{3+} - Yb^{3+}$ embedded tungsten tellurite glass, J. Lumin. (2017), http://dx.doi.org/10.1016/j.jlumin.2017.08.009.
[9] B. Ahrens, B. Henke, P.T. Miclea, J.A. Johnson, S. Schweizer, Enhanced up-converted fluorescence in fluorozirconate based glass ceramics for high efficiency solar cells, SPIE Proc. 7002 (2008) 700206–700207, http://dx.doi.org/10.1117/12.779271.
[10] S. De Niederhäusern, M. Bondi, F. Bondioli, Self-cleaning and antibacteric ceramic tile surface, Int. J. Appl. Ceram. Technol. 10 (2013) 949–956, http://dx.doi.org/10.1111/j.1744-7402.2012.02801.x.
[11] A. Bozzi, T. Yuranova, J. Kiwi, Self-cleaning of wool-polyamide and polyester textiles by TiO_2-rutile modification under daylight irradiation at ambient temperature, J. Photochem. Photobiol. A Chem. 172 (2005) 27–34, http://dx.doi.org/10.1016/j.jphotochem.2004.11.010.
[12] T. Yuranova, R. Mosteo, J. Bandara, D. Laub, J. Kiwi, Self-cleaning cotton textiles surfaces modified by photoactive SiO_2/TiO_2 coating, J. Mol. Catal. A Chem. 244 (2006) 160–167, http://dx.doi.org/10.1016/j.molcata.2005.08.059.
[13] Kaihong Qi, Xiaowen Wang, J.H. Xin, Photocatalytic self-cleaning textiles based on nanocrystalline titanium dioxide, Text. Res. J. 81 (2011) 101–110, http://dx.doi.org/10.1177/0040517510383618.
[14] J.O. Carneiro, V. Teixeira, A. Portinha, A. Magalhães, P. Coutinho, C.J. Tavares, R. Newton, Iron-doped photocatalytic TiO2 sputtered coatings on plastics for self-cleaning applications, Mater. Sci. Eng. B 138 (2007) 144–150, http://dx.doi.org/10.1016/j.mseb.2005.08.130.
[15] E.I. Cedillo-González, R. Riccò, M. Montorsi, M. Montorsi, P. Falcaro, C. Siligardi, Self-cleaning glass prepared from a commercial TiO_2 nano-dispersion and its photocatalytic performance under common anthropogenic and atmospheric factors, Build. Environ. 71 (2014) 7–14, http://dx.doi.org/10.1016/j.buildenv.2013.09.007.
[16] A. Chabas, T. Lombardo, H. Cachier, M.H. Pertuisot, K. Oikonomou, R. Falcone, M. Verità, F. Geotti-Bianchini, Behaviour of self-cleaning glass in urban atmosphere, Build. Environ. 43 (2008) 2124–2131, http://dx.doi.org/10.1016/j.buildenv.2007.12.008.
[17] B.M. Kale, J. Wiener, J. Militky, S. Rwawiire, R. Mishra, K.I. Jacob, Y. Wang, Coating of cellulose-TiO_2 nanoparticles on cotton fabric for durable photocatalytic self-cleaning and stiffness, Carbohydr. Polym. 150 (2016) 107–113, http://dx.doi.org/10.1016/j.carbpol.2016.05.006.
[18] K. Surekha, S. Sundararajan, Self-cleaning glass, Anti-Abrasive nanocoatings, Current and Future Applications, South Africa, 2015, pp. 82–103, , http://dx.doi.org/10.1016/B978-0-85709-211-3.00004-2.
[19] M.A.M.L. De Jesus, J.T.D.S. Neto, G. Timò, P.R.P. Paiva, M.S.S. Dantas, A.D.M. Ferreira, Superhydrophilic self-cleaning surfaces based on TiO_2 and TiO_2/SiO_2 composite films for photovoltaic module cover glass, Appl. Adhes. Sci. 3 (2015) 1–9, http://dx.doi.org/10.1186/s40563-015-0034-4.
[20] N.P. Mellott, C. Durucan, C.G. Pantano, M. Guglielmi, Commercial and laboratory prepared titanium dioxide thin films for self-cleaning glasses: photocatalytic performance and chemical durability, Thin Solid Films 502 (2006) 112–120, http://dx.doi.org/10.1016/j.tsf.2005.07.255.
[21] P. Thomas, Visible light driven multifunctional photocatalysis in TeO_2-based semiconductor glass ceramics, J. Photonics Energy 7 (2017) 16502, , http://dx.doi.org/10.1117/1.JPE.7.016502.

[22] A.L. da Silva, M. Dondi, D. Hotza, Self-cleaning ceramic tiles coated with Nb_2O_5-doped-TiO_2 nanoparticles, Ceram. Int. (2017), http://dx.doi.org/10.1016/j.ceramint.2017.06.049.

[23] V.A. Ganesh, H.K. Raut, A.S. Nair, S. Ramakrishna, A review on self-cleaning coatings, J. Mater. Chem. 21 (2011) 16304–16322, http://dx.doi.org/10.1039/C1JM12523K.

[24] W. Yang, X. Li, D. Chi, H. Zhang, X. Liu, Lanthanide-doped upconversion materials: emerging applications for photovoltaics and photocatalysis, Nanotechnology 25 (2014) 482001, , http://dx.doi.org/10.1088/0957-4484/25/48/482001.

[25] J. Wang, D.N. Tafen, J.P. Lewis, Z. Hong, A. Manivannan, M. Zhi, M. Li, N. Wu, Origin of photocatalytic activity of nitrogen-doped TiO_2 nanobelts, J. Am. Chem. Soc. 131 (2009) 12290–12297, http://dx.doi.org/10.1021/ja903781h.

[26] N. Wu, J. Wang, D.N. Tafen, H. Wang, J.-G. Zheng, J.P. Lewis, X. Liu, S.S. Leonard, A. Manivannan, Shape-enhanced photocatalytic activity of single-crystalline Anatase TiO_2 (101) Nanobelts, J. Am. Chem. Soc. 132 (2010) 6679–6685, http://dx.doi.org/10.1021/ja909456f.

[27] E. Thimsen, F. Le Formal, M. Gratzel, S.C. Warren, Influence of plasmonic au nanoparticles on the photoactivity of Fe_2O_3 electrodes for water splitting, Nano Lett. 11 (2011) 35–43, http://dx.doi.org/10.1021/nl1022354.

[28] T. Yang, W. Chen, Y. Hsu, K. Wei, T. Lin, T. Lin, Interfacial charge carrier dynamics in Core-shell Au-CdS nanocrystals, J. Phys. Chem. C 114 (2010) 11414–11420, http://dx.doi.org/10.1021/jp103294c.

[29] J. Tian, Y. Sang, G. Yu, H. Jiang, X. Mu, H. Liu, A Bi_2WO_6-based hybrid photocatalyst with broad spectrum photocatalytic properties under UV, visible, and near-infrared irradiation, Adv. Mater. 25 (2013) 5075–5080, http://dx.doi.org/10.1002/adma.201302014.

[30] E. Quagliarini, F. Bondioli, G.B. Goffredo, C. Cordoni, P. Munafò, Self-cleaning and de-polluting stone surfaces: TiO_2 nanoparticles for limestone, Constr. Build. Mater. 37 (2012) 51–57, http://dx.doi.org/10.1016/j.conbuildmat.2012.07.006.

[31] W. Sangchay, The self-cleaning and photocatalytic properties of TiO_2 doped with SnO_2 thin films preparation by sol-gel method, Energy Procedia 89 (2016) 170–176, http://dx.doi.org/10.1016/j.egypro.2016.05.023.

[32] M. Long, L. Zheng, B. Tan, H. Shu, Photocatalytic self-cleaning cotton fabrics with platinum (IV) chloride modified TiO_2 and N-TiO_2 coatings, Appl. Surf. Sci. 386 (2016) 434–441, http://dx.doi.org/10.1016/j.apsusc.2016.06.056.

[33] F. Gherardi, A. Colombo, M. D'Arienzo, B. Di Credico, S. Goidanich, F. Morazzoni, R. Simonutti, L. Toniolo, Efficient self-cleaning treatments for built heritage based on highly photo-active and well-dispersible TiO_2 nanocrystals, Microchem. J. 126 (2016) 54–62, http://dx.doi.org/10.1016/j.microc.2015.11.043.

[34] M.Z. Guo, A. Maury-Ramirez, C.S. Poon, Self-cleaning ability of titanium dioxide clear paint coated architectural mortar and its potential in field application, J. Clean. Prod. 112 ((2016) 3583–3588, http://dx.doi.org/10.1016/j.jclepro.2015.10.079.

[35] T. Satyanarayana, Y. Gandhi, M.A. Valente, I.V. Kityk, N. Veeraiah, Influence of titanium ions on spectroscopic properties of TeO_2-Sb_2O_3-B_2O_3: TiO_2 glass ceramics, Phys. Status Solidi Curr. Top. Solid State Phys. 8 (2011) 3082–3086, http://dx.doi.org/10.1002/pssc.201000750.

[36] L. Montagne, S. Daviero, G. Palavit, Glass network evolution with Bi^{3+}/Ti^{4+} substitution in phosphate glasses formulated with a constant oxygen/ phosphorus ratio. EXAFS, XANES, and ^{31}P double quantum MAS NMR, Am. Chem. Soc. 15 (2003) 4709–4716, http://dx.doi.org/10.1021/cm0310061.

[37] G. Lakshminarayana, R. Yang, M. Mao, J. Qiu, Spectral analysis of RE^{3+} (RE = Sm, Dy, and tm): P_2O_5-Al_2O_3-Na_2O glasses, Opt. Mater. 31 (2009) 1506–1512, http://dx.doi.org/10.1016/j.optmat.2009.02.010.

[38] G. Lakshminarayana, J. Qiu, M.G. Brik, G.A. Kumar, I.V. Kityk, Spectral analysis of Er^{3+}-, Er^{3+}/Yb^{3+}- and $Er^{3+}/Tm^{3+}/Yb^{3+}$-doped TeO_2 –ZnO–WO_3 –TiO_2 –Na_2O glasses, J. Phys. Condens. Matter 20 (2008) 375101, , http://dx.doi.org/10.1088/0953-8984/20/37/375101.

[39] N.K. Divya, P.P. Pradyumnan, Solid state synthesis of erbium doped ZnO with excellent photocatalytic activity and enhanced visible light emission, Mater. Sci. Semicond. Process. 41 (2016) 428–435, http://dx.doi.org/10.1016/j.mssp.2015.10.004.

[40] N. Prakash, R. Karthikeyan, D. Thangaraju, M. Navaneethan, M. Arivanandhan, T. Koyama, Y. Hayakawa, Effect of erbium on the photocatalytic activity of TiO_2/Ag nanocomposites under visible light irradiation, ChemPhysChem 16 (2015) 3084–3092, http://dx.doi.org/10.1002/cphc.201500492.

[41] S. Obregón, G. Colón, Evidence of upconversion luminescence contribution to the improved photoactivity of erbium doped TiO_2 systems, Chem. Commun. 48 (2012) 7865, http://dx.doi.org/10.1039/c2cc33391k.

[42] A. Awang, S.K. Ghoshal, M.R. Sahar, R. Arifin, F. Nawaz, Non-spherical gold nanoparticles mediated surface plasmon resonance in Er^{3+} doped zinc-sodium tellurite glasses: role of heat treatment, J. Lumin. 149 (2014) 138–143, http://dx.doi.org/10.1016/j.jlumin.2014.01.027.

[43] S.K. Ghoshal, A. Awang, M.R. Sahar, R. Arifin, Gold nanoparticles assisted surface enhanced Raman scattering and luminescence of Er^{3+} doped zinc–sodium tellurite glass, J. Lumin. 159 (2015) 265–273, http://dx.doi.org/10.1016/j.jlumin.2014.11.032.

[44] M.R. Dousti, Spectroscopoc and structural properties of TeO_2-ZnO-Na_2O-Er_2O_3-Au glasses, Chalcogenide Lett. 10 (2013) 411–420.

[45] M. Sakhuja, J. Son, H. Yang, C.S. Bhatia, A.J. Danner, Outdoor performance and durability testing of antireflecting and self-cleaning glass for photovoltaic applications, Sol. Energy 110 (2014) 231–238, http://dx.doi.org/10.1016/j.solener.2014.07.003.

[46] X. Zhao, Q. Zhao, J. Yu, B. Liu, Development of multifunctional photoactive self-cleaning glasses, J. Non-Cryst. Solids 354 (2008) 1424–1430, http://dx.doi.org/10.1016/j.jnoncrysol.2006.10.093.

[47] L.K. Verma, M. Sakhuja, J. Son, A.J. Danner, H. Yang, H.C. Zeng, C.S. Bhatia, Self-cleaning and antireflective packaging glass for solar modules, Renew. Energy 36 (2011) 2489–2493, http://dx.doi.org/10.1016/j.renene.2011.02.017.

[48] M. Saad, M. Poulain, Glass forming ability criterion, Mater. Sci. Forum 19–20 (1987) 11–18, http://dx.doi.org/10.4028/www.scientific.net/MSF.19-20.11.

[49] V. Dimitrov, S. Sakka, Linear and nonlinear optical properties of simple oxides. II, J. Appl. Phys. 79 (1996) 1741, http://dx.doi.org/10.1063/1.360963.

[50] L. Lorenz, On the thermal and electrical conductivities of metals, Ann. Phys. 249 (1881) 422–447.

[51] N.F. Mott, E.A. Davis, Electronic Processes in Non Crystalline Materials, 2nd ed., Clarendon Press, United Kingdom, 1979.

[52] H. Gu, C. Wang, S. Gong, Y. Mei, H. Li, W. Ma, Investigation on contact angle measurement methods and wettability transition of porous surfaces, Surf. Coat. Technol. 292 (2016) 72–77, http://dx.doi.org/10.1016/j.surfcoat.2016.03.014.

[53] R.N. Wenzel, Resistance of solid surfaces to wetting by water, J. Ind. Eng. Chem. 28 (1936) 988–994, http://dx.doi.org/10.1021/ie50320a024.

[54] M. Schroder, Work of adhesion of a sessile drop to a clean surface, J. Colloid Interface Sci. 213 (1999) 602–605, http://dx.doi.org/10.1006/jcis.1999.6148.

[55] M.E. Schrader, Young-dupre revisited, Langmuir 11 (1995) 3585–3589, http://dx.doi.org/10.1021/la00009a049.

[56] D. Subedi, Contact angle measurement for the surface characterization of solids, Himal. Phys. (2011) 1–4, http://dx.doi.org/10.1073/pnas.1201800109.

[57] J.E. George, S. Chidangil, S.D. George, A study on air bubble wetting: role of surface wettability, surface tension, and ionic surfactants, Appl. Surf. Sci. 410 (2017) 117–125, http://dx.doi.org/10.1016/j.apsusc.2017.03.071.

[58] E.M. Baba, C.E. Cansoy, E.O. Zayim, Optical and wettability properties of polymers with varying surface energies, Appl. Surf. Sci. 350 (2015) 115–120, http://dx.doi.org/10.1016/j.apsusc.2015.02.150.

[59] R. Blossey, Self-cleaning surfaces — virtual realities, Nat. Mater. 2 (2003) 301–306, http://dx.doi.org/10.1038/nmat856.

[60] K. Yao, P. Basnet, H. Sessions, G.K. Larsen, S.E.H. Murph, Y. Zhao, Fe_2O_3-TiO_2 core-shell nanorod arrays for visible light photocatalytic applications, Catal. Today 270 (2016) 51–58, http://dx.doi.org/10.1016/j.cattod.2015.10.026.

[61] I. Soltani, S. Hraiech, K. Horchani-naifer, H. Elhouichet, M. Férid, Effect of silver nanoparticles on spectroscopic properties of Er^{3+} doped phosphate glass, Opt. Mater. 46 (2015) 1–7, http://dx.doi.org/10.1016/j.optmat.2015.05.003.

[62] B. Ingham, T.H. Lim, C.J. Dotzler, A. Henning, M.F. Toney, R.D. Tilley, How nanoparticles coalesce: an in situ study of au nanoparticle aggregation and grain growth, Chem. Mater. 23 (2011) 3312–3317, http://dx.doi.org/10.1021/cm200354d.

[63] T. Som, B. Karmakar, Synthesis and enhanced photoluminescence in novel Au core Au – Ag shell nanoparticles embedded Nd^{3+} – doped antimony oxide glass hybrid nanocomposites, J. Quant. Spectrosc. Radiat. Transf. 112 (2011) 2469–2479, http://dx.doi.org/10.1016/j.jqsrt.2011.06.015.

[64] P. Cheng, Y. Zhou, M. Zhou, X. Su, Z. Zhou, G. Yang, Enhanced broadband near-infrared luminescence from Pr^{3+}-doped tellurite glass with silver nanoparticles, Opt. Mater. 73 (2017) 102–110, http://dx.doi.org/10.1016/j.optmat.2017.07.044.

[65] Z. Zhou, Y. Zhou, M. Zhou, X. Su, P. Cheng, The enhanced near-infrared fluorescence of Nd $^{3+}$-doped tellurite glass, J. Non-Cryst. Solids (2017) 0–1, http://dx.doi.org/10.1016/j.jnoncrysol.2017.05.005.

[66] M. Cai, Y. Lu, R. Cao, Y. Tian, S. Xu, J. Zhang, 2 μm emission properties and hydroxy groups quenching of Tm^{3+} in germanate-tellurite glass, Opt. Mater. 57 (2016) 236–242, http://dx.doi.org/10.1016/j.optmat.2016.03.055.

[67] M. Anand Pandarinath, G. Upender, K. Narasimha Rao, D. Suresh Babu, Thermal, optical and spectroscopic studies of boro-tellurite glass system containing ZnO, J. Non-Cryst. Solids 433 (2016) 60–67, http://dx.doi.org/10.1016/j.jnoncrysol.2015.11.028.

[68] V. Sreenivasulu, G. Upender, V.V. Priya Swapna, V.C. Mouli, M. Prasad, Raman, DSC, ESR and optical properties of lithium cadmium zinc tellurite glasses, Phys. B Condens. Matter 454 (2014) 60–66, http://dx.doi.org/10.1016/j.physb.2014.06.039.

[69] Y. Tian, B. Li, R. Chen, J. Xia, X. Jing, J. Zhang, S. Xu, Thermal stability and 2.7 μm spectroscopic properties in Er^{3+} doped tellurite glasses, Solid State Sci. 60 (2016) 17–22, http://dx.doi.org/10.1016/j.solidstatesciences.2016.07.012.

[70] M. Ahamed, M.A.M. Khan, M.J. Akhtar, H.A. Alhadlaq, A. Alshamsan, Role of Zn doping in oxidative stress mediated cytotoxicity of TiO2 nanoparticles in human breast cancer MCF-7 cells, Sci Rep 6 (2016) 30196, , http://dx.doi.org/10.1038/srep30196.

[71] F. Behafarid, B.R. Cuenya, Coarsening phenomena of metal nanoparticles and the influence of the support pre-treatment: Pt/TiO_2(110), Surf. Sci. 606 (2012) 908–918, http://dx.doi.org/10.1016/j.susc.2012.01.022.

[72] S.A.M. Azmi, M.R. Sahar, S.K. Ghoshal, R. Arifin, Modification of structural and physical properties of samarium doped zinc phosphate glasses due to the inclusion of nickel oxide nanoparticles, J. Non-Cryst. Solids 411 (2015) 53–58, http://dx.doi.org/10.1016/j.jnoncrysol.2014.12.024.

[73] T. Hawa, M.R. Zachariah, Coalescence kinetics of unequal sized nanoparticles, J. Aerosol Sci. 37 (2006) 1–15, http://dx.doi.org/10.1016/j.jaerosci.2005.02.007.

[74] N.M. Yusoff, M.R. Sahar, Effect of silver nanoparticles incorporated with samarium-doped magnesium tellurite glasses, Phys. B Condens. Matter 456 (2015) 191–196, http://dx.doi.org/10.1016/j.physb.2014.08.039.

[75] G.H.A. Melo, J.D.M. Dias, T.A. Lodi, M.J. Barboza, F. Pedrochi, A. Steimacher, Optical and spectroscopic properties of Eu_2O_3 doped CaBAl glasses, Opt. Mater. 54 (2016) 98–103, http://dx.doi.org/10.1016/j.optmat.2016.02.015.

[76] M. Abdel-Baki, F. El-Diasty, F.A.A. Wahab, Optical characterization of $x$$TiO_2$–(60 s − x)SiO_2–40Na_2O glasses: II. Absorption edge, fermi level, electronic

polarizability and optical basicity, Opt. Commun. 261 (2006) 65–70, http://dx.doi.org/10.1016/j.optcom.2005.11.056.
[77] M. Abdel-Baki, F. El-Diasty, Optical properties of oxide glasses containing transition metals: case of titanium- and chromium-containing glasses, Curr. Opin. Solid State Mater. Sci. 10 (2006) 217–229, http://dx.doi.org/10.1016/j.cossms.2007.08.001.
[78] Z. Ashur Said Mahraz, M.R. Sahar, S.K. Ghoshal, M.R. Dousti, R.J. Amjad, Silver nanoparticles enhanced luminescence of Er^{3+} ions in boro-tellurite glasses, Mater. Lett. 112 (2013) 136–138, http://dx.doi.org/10.1016/j.matlet.2013.08.131.
[79] Z.A. Said Mahraz, M.R. Sahar, S.K. Ghoshal, Band gap and polarizability of boro-tellurite glass: influence of erbium ions, J. Mol. Struct. 1072 (2014) 238–241, http://dx.doi.org/10.1016/j.molstruc.2014.05.017.
[80] M.N. Azlan, M.K. Halimah, S.Z. Shafinas, W. Daud, Electronic polarizability of zinc borotellurite glass system containing erbium nanoparticles, Mater. Express 5 (2015) 211–218, http://dx.doi.org/10.1166/mex.2015.1236.
[81] Z.A. Said Mahraz, M.R. Sahar, S.K. Ghoshal, M. Reza Dousti, Concentration dependent luminescence quenching of Er^{3+}-doped zinc boro-tellurite glass, J. Lumin. 144 (2013) 139–145, http://dx.doi.org/10.1016/j.jlumin.2013.06.050.
[82] S.F. Ismail, M.R. Sahar, S.K. Ghoshal, Physical and absorption properties of titanium nanoparticles incorporated into zinc magnesium phosphate glass, Mater. Charact. 111 (2016) 177–182, http://dx.doi.org/10.1016/j.matchar.2015.11.030.
[83] I. Jlassi, H. Elhouichet, M. Ferid, R. Chtourou, M. Oueslati, Study of photoluminescence quenching in Er^{3+}-doped tellurite glasses, Opt. Mater. 32 (2010) 743–747, http://dx.doi.org/10.1016/j.optmat.2010.02.006.
[84] M.K. Halimah, W.M. Daud, H.A.A. Sidek, A.W. Zaidan, A.S. Zainal, Optical properties of ternary tellurite glasses, Mater. Sci. Pol. 28 (2010) 173–180.
[85] K. Guan, Relationship between photocatalytic activity, hydrophilicity and self-cleaning effect of TiO_2/SiO_2 films, Surf. Coat. Technol. 191 (2005) 155–160, http://dx.doi.org/10.1016/j.surfcoat.2004.02.022.
[86] L.R. Sonders, D.P. Enright, W.A. Weyl, Wettability, a function of the polarizability of the surface ions, J. Appl. Phys. 21 (1950) 338–344, http://dx.doi.org/10.1063/1.1699665.
[87] Y.M. Kim, B. Arkles, Y. Pan, The Role Of Polarity In The Structure Of Silanes Employed In Surface Modification, Silanes Other Coupling Agents, Vol. 5, (2009), pp. 51–64, http://dx.doi.org/10.1163/ej.9789004165915.i-348.37.
[88] H. Nurhafizah, M.S. Rohani, S.K. Ghoshal, Self Cleanliness of Er^{3+}/Nd^{3+} co-doped lithium niobate Tellurite Glass Containing Silver Nanoparticles, (2016), http://dx.doi.org/10.1016/j.jnoncrysol.2016.10.028.
[89] S.F. Ismail, M.R. Sahar, S.K. Ghoshal, Effects of titanium nanoparticles on self-cleaning and structural features of zinc-magnesium-phosphate glass, Mater. Res. Bull. 74 (2016) 502–506, http://dx.doi.org/10.1016/j.materresbull.2015.11.022.
[90] I.P. Parkin, R.G. Palgrave, Self-cleaning coatings, J. Mater. Chem. 15 (2005) 1689, http://dx.doi.org/10.1039/b412803f.
[91] S.R. Saad, N. Mahmed, M.M.A.B. Abdullah, A.V. Sandu, Self-cleaning technology in fabric: a review, Conf. Ser. Mater. Sci. Eng. 133 (2016) 12028, , http://dx.doi.org/10.1088/1757-899X/133/1/012028.
[92] B. Zahiri, P.K. Sow, C.H. Kung, W. Mérida, Active control over the wettability from superhydrophobic to superhydrophilic by electrochemically altering the oxidation state in a low voltage range, Adv. Mater. Interfaces 4 (2017) 1–12, http://dx.doi.org/10.1002/admi.201700121.
[93] S.K. Rhee, Surface energies of silicate glasses calculated from their wettability data, J. Mater. Sci. 12 (1977) 823–824, http://dx.doi.org/10.1007/BF00548176.
[94] K. Boyd, H. Ebendorff-Heidepriem, T.M. Monro, J. Munch, Surface tension and viscosity measurement of optical glasses using a scanning CO_2 laser, Opt. Mater. Express. 2 (2012) 1101, http://dx.doi.org/10.1364/OME.2.001101.
[95] E.A. Abou Neel, I. Ahmed, J.J. Blaker, A. Bismarck, A.R. Boccaccini, M.P. Lewis, S.N. Nazhat, J.C. Knowles, Effect of iron on the surface, degradation and ion release properties of phosphate-based glass fibres, Acta Biomater. 1 (2005) 553–563, http://dx.doi.org/10.1016/j.actbio.2005.05.001.
[96] E.A. Abou Neel, W. Chrzanowski, J.C. Knowles, Effect of increasing titanium dioxide content on bulk and surface properties of phosphate-based glasses, Acta Biomater. 4 (2008) 523–534, http://dx.doi.org/10.1016/j.actbio.2007.11.007.
[97] J. Chung, B. Ryu, Crystallization behavior of phosphate glasses with hydrophobic coating materials, J. Nanomater. 2015 (2015), http://dx.doi.org/10.1155/2015/981720.
[98] H.L. Skriver, N.M. Rosengaard, Surface energy and work function of elemental metals, Phys. Rev. B 46 (1992) 7157–7168, http://dx.doi.org/10.1103/PhysRevB.46.7157.
[99] D.Y. Lee, M.-H. Lee, N.-I. Cho, Preparation and photocatalytic degradation of erbium doped titanium dioxide nanorods, Curr. Appl. Phys. 12 (2012) 1229–1233, http://dx.doi.org/10.1016/j.cap.2012.03.007.
[100] D. Dijkhuis, Mass Transfer in Titania Photocatalytic Membrane Reactors, (2017).
[101] P. Cheng, Y. Zhou, X. Su, M. Zhou, Z. Zhou, The near-infrared band luminescence in silver NPs embedded tellurite glass doped with $Er^{3+}/Tm^{3+}/Yb^{3+}$ ions, J. Alloys Compd. 714 (2017) 370–380, http://dx.doi.org/10.1016/j.jallcom.2017.04.067.
[102] P. Pichat, Photocatalysis and Water Purification: From Fundamentals to Recent Applications, (2013), http://dx.doi.org/10.1002/9783527645404.
[103] S. Banerjee, D.D. Dionysiou, S.C. Pillai, Self-cleaning applications of TiO_2 by photo-induced hydrophilicity and photocatalysis, Appl. Catal. B Environ. 176–177 (2015) 396–428, http://dx.doi.org/10.1016/j.apcatb.2015.03.058.
[104] N. Xu, Z. Shi, Y. Fan, J. Dong, J. Shi, M.Z.-C. Hu, Effects of particle size of TiO_2 on photocatalytic degradation of methylene blue in aqueous suspensions, Ind. Eng. Chem. Res. 38 (1999) 373–379, http://dx.doi.org/10.1021/ie980378u.
[105] S.Y. Kim, T.H. Lim, T.S. Chang, C.H. Shin, Photocatalysis of methylene blue on titanium dioxide nanoparticles synthesized by modified sol-hydrothermal process of TiCl4, Catal. Lett. 117 (2007) 112–118, http://dx.doi.org/10.1007/s10562-007-9115-8.
[106] D. Yin, L. Zhang, X. Cao, J. Tang, W. Huang, Y. Han, Y. Liu, T. Zhang, M. Wu, Improving photocatalytic activity by combining upconversion nanocrystals and Mo-doping: a case study on β-$NaLuF_4$:Gd,Yb,Tm@SiO_2@TiO_2:Mo, RSC Adv. (2015) 86849–87738, http://dx.doi.org/10.1039/C5RA12852H.
[107] T. Yoko, Coordination of Ti^{4+} and Ge^{4+} ions in Na_2O-TiO_2-GeO_2 glasses an approach based on crystallization behaviour, X-ray absorption and I R spectroscopy, J. Mater. Sci. 20 (1985) 906–916.
[108] J. Tian, X. Hu, H. Yang, Y. Zhou, H. Cui, H. Liu, High yield production of reduced TiO_2 with enhanced photocatalytic activity, Appl. Surf. Sci. 360 ((2016) 738–743, http://dx.doi.org/10.1016/j.apsusc.2015.11.056.
[109] D. Qi, L. Lu, Z. Xi, L. Wang, J. Zhang, Enhanced photocatalytic performance of TiO_2 based on synergistic effect of Ti^{3+} self-doping and slow light effect, Appl. Catal. B Environ. 160–161 (2014) 621–628, http://dx.doi.org/10.1016/j.apcatb.2014.06.020.
[110] Z. Wan, G.-F. Huang, W.-Q. Huang, C. Jiao, X.-G. Yan, Z.-M. Yang, Q. Zhang, The enhanced photocatalytic activity of Ti^{3+} self-doped TiO_2 by a reduction method, Mater. Lett. 122 (2014) 33–36, http://dx.doi.org/10.1016/j.matlet.2014.01.181.
[111] Y. Zhu, M.W. Shah, C. Wang, Insight into the role of Ti^{3+} in photocatalytic performance of shuriken-shaped $BiVO_4/TiO_{2-x}$ heterojunction, Appl. Catal. B Environ. 203 (2017) 526–532, http://dx.doi.org/10.1016/j.apcatb.2016.10.056.
[112] V.C. Bhethanabotla, D.R. Russell, J.N. Kuhn, Assessment of mechanisms for enhanced performance of Yb/Er/titania photocatalysts for organic degradation: role of rare earth elements in the titania phase, Appl. Catal. B Environ. 202 (2017) 156–164, http://dx.doi.org/10.1016/j.apcatb.2016.09.008.
[113] Y. Zhou, Y. Liu, P. Liu, W. Zhang, M. Xing, J. Zhang, A facile approach to further improve the substitution of nitrogen into reduced TiO_{2-x} with an enhanced photocatalytic activity, Appl. Catal. B Environ. 170–171 (2015) 66–73, http://dx.doi.org/10.1016/j.apcatb.2015.01.036.
[114] A. Fujishima, X. Zhang, D.A. Tryk, TiO_2 photocatalysis and related surface phenomena, Surf. Sci. Rep. 63 (2008) 515–582, http://dx.doi.org/10.1016/j.surfrep.2008.10.001.
[115] Y. Qu, X. Duan, Progress, challenge and perspective of heterogeneous photocatalysts, Chem. Soc. Rev. 42 (2013) 2568–2580, http://dx.doi.org/10.1039/C2CS35355E.
[116] Y. Chen, W. Li, J. Wang, Y. Gan, L. Liu, M. Ju, Microwave-assisted ionic liquid synthesis of Ti^{3+} self-doped TiO_2 hollow nanocrystals with enhanced visible-light photoactivity, Appl. Catal. B Environ. 191 (2016) 94–105, http://dx.doi.org/10.1016/j.apcatb.2016.03.021.
[117] J. Wang, F.Y. Wen, Z.H. Zhang, X.D. Zhang, Z.J. Pan, P. Zhang, P.L. Kang, J. Tong, L. Wang, L. Xu, Investigation on degradation of dyestuff wastewater using visible light in the presence of a novel nano TiO_2 catalyst doped with upconversion luminescence agent, J. Photochem. Photobiol. A Chem. 180 (2006) 189–195, http://dx.doi.org/10.1016/j.jphotochem.2005.10.016.
[118] F. Ahmadi, R. Hussin, S.K. Ghoshal, Spectral characteristics of Er^{3+} doped magnesium zinc sulfophosphate glasses, J. Alloys Compd. 711 (2017) 94–102, http://dx.doi.org/10.1016/j.jallcom.2017.03.212.
[119] L.C. Oliveira, A. Marcus, N. Lima, C. Thirstrup, H.F. Neff, Surface Plasmon Resonance Sensors A Materials Guide to Design and Optimization, Springer, New York, 2015, http://dx.doi.org/10.1007/978-3-319-14926-4.
[120] D. Harvey, Modern analytical chemistry, J. Chem. Inf. Model. 53 (2013) 1689–1699, http://dx.doi.org/10.1017/CBO9781107415324.004.
[121] M.S. Sajna, S. Thomas, K.A. Ann Mary, C. Joseph, P.R. Biju, N.V. Unnikrishnan, Spectroscopic properties of Er^{3+} ions in multicomponent tellurite glasses, J. Lumin. 159 (2015) 55–65, http://dx.doi.org/10.1016/j.jlumin.2014.10.062.
[122] H. Fares, H. Elhouichet, B. Gelloz, M. Férid, Silver nanoparticles enhanced luminescence properties of Er^{3+} doped tellurite glasses: effect of heat treatment, J. Appl. Phys. 116 (2014) 123504, , http://dx.doi.org/10.1063/1.4896363.
[123] A. Langar, C. Bouzidi, H. Elhouichet, M. Férid, Er-Yb codoped phosphate glasses with improved gain characteristics for an efficient 1.55 μm broadband optical amplifiers, J. Lumin. 148 (2014) 249–255, http://dx.doi.org/10.1016/j.jlumin.2013.12.008.
[124] H. Fares, H. Elhouichet, B. Gelloz, M. Férid, Surface plasmon resonance induced Er^{3+} photoluminescence enhancement in tellurite glass, J. Appl. Phys. 117 (2015) 193102, , http://dx.doi.org/10.1063/1.4921436.
[125] Y. Qi, Y. Zhou, L. Wu, F. Yang, S. Peng, S. Zheng, D. Yin, Silver nanoparticles enhanced 1.53 μm band fluorescence of Er^{3+}/Yb^{3+} codoped tellurite glasses, J. Lumin. 153 (2014) 401–407, http://dx.doi.org/10.1016/j.jlumin.2014.03.069.
[126] G. Upender, S. Bharadwaj, A.M. Awasthi, V. Chandra Mouli, Glass transition temperature-structural studies of tungstate tellurite glasses, Mater. Chem. Phys. 118 (2009) 298–302, http://dx.doi.org/10.1016/j.matchemphys.2009.07.058.
[127] K. Venkata Krishnaiah, J. Marques-Hueso, K. Suresh, G. Venkataiah, B.S. Richards, C.K. Jayasankar, Spectroscopy and near infrared upconversion of Er^{3+}-doped TZNT glasses, J. Lumin. 169 ((2016) 270–276, http://dx.doi.org/10.1016/j.jlumin.2015.08.035.
[128] S. Marjanovic, J. Toulouse, H. Jain, C. Sandmann, V. Dierolf, A.R. Kortan, N. Kopylov, R.G. Ahrens, Characterization of new erbium-doped tellurite glasses and fibers, J. Non-Cryst. Solids 322 (2003) 311–318, http://dx.doi.org/10.1016/S0022-3093(03)00278-3.
[129] G. Guery, A. Fargues, T. Cardinal, M. Dussauze, F. Adamietz, V. Rodriguez, J.D. Musgraves, K. Richardson, P. Thomas, Impact of tellurite-based glass structure on Raman gain, Chem. Phys. Lett. 554 (2012) 123–127, http://dx.doi.org/10.1016/j.cplett.2012.10.023.
[130] E. Le Ru, P. Etchegoin, Principles of surface enhanced Raman, Spectroscopy (2014), http://dx.doi.org/10.1007/s13398-014-0173-7.2.

[131] H. Sharma, D.C. Agarwal, A.K. Shukla, D.K. Avasthi, V.D. Vankar, Surface-enhanced Raman scattering and fluorescence emission of gold nanoparticle-multi-walled carbon nanotube hybrids, J. Raman Spectrosc. 44 (2013) 12–20, http://dx.doi.org/10.1002/jrs.4136.

[132] W. Yu, X. Liu, L. Pan, J. Li, J. Liu, J. Zhang, P. Li, C. Chen, Z. Sun, Enhanced visible light photocatalytic degradation of methylene blue by F-doped TiO_2, Appl. Surf. Sci. 319 (2014) 107–112, http://dx.doi.org/10.1016/j.apsusc.2014.07.038.

[133] L. Basse, J.L. Hansen, P.B. Jensen, B. Julsgaard, Erbium diffusion in titanium dioxide, AIP Adv. 7 (2017) 1–7, http://dx.doi.org/10.1063/1.4979923.

[134] M. Sakhuja, J. Son, H. Yang, C.S. Bhatia, A.J. Danner, Outdoor performance and durability testing of antireflecting and self-cleaning glass for photovoltaic applications, Sol. Energy 110 (2014) 231–238, http://dx.doi.org/10.1016/j.solener.2014.07.003.